

# Atmospheric photooxidation and ozonolysis of sabinene: Reaction rate coefficients, product yields and chemical budget of radicals

Jacky Y. S. Pang<sup>1</sup>, Florian Berg<sup>1</sup>, Anna Novelli<sup>1</sup>, Birger Bohn<sup>1</sup>, Michelle Färber<sup>1</sup>, Philip T. M. Carlsson<sup>1</sup>, René Dubus<sup>1</sup>, Georgios I. Gkatzelis<sup>1</sup>, Franz Rohrer<sup>1</sup>, Sergej Wedel<sup>1</sup>, Andreas Wahner<sup>1</sup>, and Hendrik Fuchs<sup>1,2</sup>

<sup>1</sup>Institute of Energy and Climate Research, IEK-8: Troposphere, Forschungszentrum Jülich GmbH, Jülich, Germany

<sup>2</sup>Department of Physics, University of Cologne, Cologne, Germany

*Correspondence to:* Hendrik Fuchs (h.fuchs@fz-juelich.de)

**Abstract.** The oxidation of sabinene by the hydroxyl radical (OH) and ozone (O<sub>3</sub>) was investigated under atmospherically relevant conditions in the atmospheric simulation chamber SAPHIR at Forschungszentrum Jülich, Germany. The rate coefficients of the reactions of sabinene with OH and with O<sub>3</sub> were determined. The temperature dependence between 284 K to 340 K of the rate coefficient of the reaction of sabinene with OH,  $k_{\text{SAB+OH}}$ , was measured for the first time using an OH reactivity instrument, resulting in an Arrhenius expression of  $(1.67 \pm 0.16) \times 10^{-11} \times \exp((575 \pm 30)/T) \text{ cm}^3 \text{ s}^{-1}$ . The values agree with those determined in chamber experiments in this work and reported in the literature for ~298 K within the uncertainties of measurements. The ozonolysis reaction rate coefficient of sabinene ( $k_{\text{SAB+O}_3}$ ) determined in chamber experiments at a temperature of  $(278 \pm 2) \text{ K}$  is  $(3.4 \pm 0.8) \times 10^{-17} \text{ cm}^3 \text{ s}^{-1}$ , which is 58 % lower than the value reported in the literature for room temperature. The measurement of products from the oxidation of sabinene by OH resulted in an acetone yield of  $(21 \pm 15) \%$ , a formaldehyde yield of  $(46 \pm 25) \%$ , and a sabinaketone yield of  $(18 \pm 16) \%$ . All yields determined in the chamber experiments agree well with values from previous laboratory studies within their uncertainties. In addition, the formaldehyde yield determined in this study is consistent with that predicted by the sabinene OH-oxidation mechanism which was devised from quantum chemical calculations by Wang and Wang (2018), whereas the acetone yield is about 15 % absolute higher than that predicted by the mechanism. In the ozonolysis experiments, the analysis of product measurements results in an acetone yield of  $(5 \pm 2) \%$ , a formaldehyde yield of  $(48 \pm 15) \%$ , a sabinaketone yield of  $(31 \pm 15) \%$ , and an OH radical yield of  $(26 \pm 29) \%$ . The OH radical yield is lower than expected from the theoretical mechanism in Wang and Wang (2017), but the value still agrees within the uncertainty. An analysis of the chemical budget of OH radicals was performed for the chamber experiments. The analysis reveals that the destruction rate of OH radical matches the production rate of OH suggesting that there is no significant missing OH source for example from isomerization reactions of peroxy radicals for the experimental conditions in this work.

## 1 Introduction

30 Monoterpenes are an important constituent of biogenic volatile organic compounds (BVOCs). About 160 Tg of monoterpenes are released into the atmosphere each year (Guenther et al., 2012). They play an important role in tropospheric chemistry and the formation of secondary pollutions such as ozone (O<sub>3</sub>) and particles due to their high reactivity toward major oxidants in the atmosphere that include hydroxyl radicals (OH), O<sub>3</sub> and nitrate radicals (NO<sub>3</sub>) (Atkinson and Arey, 2003). Sabinene contributes up to 7 % to the total monoterpene emissions and is the 5<sup>th</sup>-most abundant monoterpene species in the atmosphere  
35 (Sindelarova et al., 2014). Sabinene is for example emitted by beech (Tollsten and Müller, 1996), birch (Hakola et al., 1998), and oak trees (Staudt and Bertin, 1998), making sabinene the major monoterpene emission in some European (Hakola et al., 2003; Holzke et al., 2006) and Asian forests (Kim et al., 2005).

The chemical structure of sabinene is similar to that of  $\beta$ -pinene, a monoterpene with an exocyclic C-C double bond and bicyclic rings. The oxidation of  $\beta$ -pinene has been extensively investigated in many laboratory (e.g., Kaminski et al., 2017; Xu  
40 et al., 2019) and theoretical studies (e.g., Nguyen et al., 2009; Vereecken and Peeters, 2012), while only a few studies have been performed with sabinene. Sabinene differs from  $\beta$ -pinene by having a three-membered bridging ring instead of a four-membered ring. The lower number of carbon atom in the bicyclic ring of sabinene leads to a higher strain in the ring impacting the reaction pathways in the oxidation of sabinene.

Organic peroxy radicals (RO<sub>2</sub>) are formed upon the oxidation by OH radicals and O<sub>3</sub>. The subsequent chemistry of the RO<sub>2</sub>  
45 radicals depends mostly on the availability of nitric oxide (NO) in the atmosphere as NO rapidly reacts with RO<sub>2</sub> radicals, so that other reaction pathways often cannot compete. In addition to bimolecular reactions, some RO<sub>2</sub> radicals can undergo unimolecular reactions that are competitive with bimolecular reactions in environments with low NO mixing ratios (< 1 ppbv) such as forests. The position of functional groups in the RO<sub>2</sub> radical affects the rate of unimolecular reactions (Vereecken and Nozière, 2020). Unimolecular RO<sub>2</sub> reactions can lead to the regeneration of OH radicals and therefore enhance the self-cleansing ability of the atmosphere. This is for example known for RO<sub>2</sub> radicals produced from isoprene and methacrolein  
50 (e.g., da Silva et al., 2010; Crouse et al., 2011, 2012; Fuchs et al., 2013, 2014; Peeters et al., 2014; Novelli et al., 2020), which partly explains the deficit in the OH production rate found in field experiments in isoprene-rich environments at low NO concentrations (Lelieveld et al., 2008; Whalley et al., 2011). The exact fate of RO<sub>2</sub> radicals in their subsequent chemistry determines the distribution of oxidation products and the yield of secondary organic aerosol.

55 There are only a few studies investigating specifically the chemical budget of radicals in the oxidation chain of monoterpenes. The available literature indicates that current chemical models underestimate the formation of hydroperoxyl radicals (HO<sub>2</sub>) in the photooxidation of  $\alpha$ -pinene and  $\beta$ -pinene (Kaminski et al., 2017; Rolletter et al., 2019). There has been no study investigating the chemical budget of radicals in the oxidation of sabinene.

In this study, the oxidation of sabinene by OH and O<sub>3</sub> was investigated in experiments in the atmospheric simulation chamber  
60 SAPHIR (Simulation of Atmospheric Photochemistry In a Large Reaction Chamber) at Forschungszentrum Jülich, Germany.

Experiments were performed at ambient conditions with the aim to improve the understanding of the oxidation mechanism of sabinene, which included the determination of reaction rate coefficients with oxidants (OH and O<sub>3</sub>), product yields (acetone, formaldehyde, and OH from the ozonolysis reaction) and the chemical budget of OH radicals. Additional measurements were performed in the laboratory to determine the temperature dependence of the rate coefficient of the reaction of sabinene with  
65 OH radicals.

## 2 Oxidation mechanism of sabinene

There are only a few experimental and theoretical studies on the oxidation mechanism of sabinene and to the best of our knowledge a detailed oxidation mechanism of sabinene including the subsequent chemistry of oxidation products is not available (Carrasco et al., 2006; Wang and Wang, 2017, 2018; Almatrneh et al., 2019). Figure 1 and Figure 2 show the current  
70 knowledge of the oxidation mechanisms of sabinene by OH (Wang and Wang, 2018) and O<sub>3</sub> (Wang and Wang, 2017), respectively, derived from quantum chemical calculations.

In the theoretical calculations conducted by Wang and Wang (2017 and 2018), molecular structures were first optimized and the vibrational frequencies were calculated at M06-2X/6-311++G(2df,2p) level. Electronic energies were calculated by wave function (UCBS-QB3) for the OH-oxidation of sabinene and at the RHF-UCCSD(T)-F12a level for the sabinene ozonolysis  
75 reaction. High-pressure limit rate coefficients were determined using the canonical transition state theory, whereas fast unimolecular reactions and their dependence on pressure and temperature were calculated with master equations (RRKM-ME) using Mesmer and MultiWell-2017 codes.

In the reaction with OH, sabinene either undergoes hydrogen abstraction or OH addition at the exocyclic C-C double bond. OH addition is predicted to be the dominant pathway from structure-activity relationships (SAR) (Peeters et al., 2007) and  
80 quantum chemical calculations (Wang and Wang, 2018). Several alkyl radical isomers can be produced from the H-abstraction reaction, but their total yield is only 4 % to 8 % (reaction path (c) in Fig. 1). OH-addition to the cyclic carbon results in a primary alkyl radical with a yield of 47 % (reaction path (a) in Fig. 1) and addition to the terminal carbon results in a tertiary alkyl radical with a yield of 45 % (reaction path (b) in Fig. 1). Yields are derived from the energy barrier of the OH addition reactions in the quantum chemical calculations by Wang and Wang (2018). It is worth noting that the OH-addition at the cyclic  
85 carbon is much more favorable in sabinene than in  $\beta$ -pinene, for which the yield of the primary alkyl radical from the OH addition to the cyclic carbon atom is only 8 % and the yield of the tertiary alkyl radical from the OH addition to the terminal carbon atom is 92 %.

After the addition of OH, the tertiary alkyl radical quickly isomerizes by breaking the three-membered ring resulting in a RO<sub>2</sub> radical (SABINOHBO<sub>2</sub>, Fig. 1) after the reaction with oxygen molecules (O<sub>2</sub>). The ring-opening reaction is faster than the  
90 immediate addition of O<sub>2</sub> under atmospheric conditions resulting in a yield of 99 % of RO<sub>2</sub> radical SABINOHBO<sub>2</sub> (Wang and Wang, 2018). The impact of strain in the 3-membered ring is apparent when comparing the yield of the ring-opening RO<sub>2</sub>

radical SABINOHBO2 to the analogous ring-opening RO<sub>2</sub> radical from the OH-oxidation of β-pinene that has a 4-membered ring. In the case of β-pinene, ring-opening is less competitive than the immediate O<sub>2</sub> addition and the yield of the ring-opening RO<sub>2</sub> radical is only 30 % (Vereecken and Peeters, 2012).

95 The RO<sub>2</sub> radical SABINOHBO2 can either further react in bimolecular reactions like other organic RO<sub>2</sub> radicals (e.g., with NO) forming eventually a hydroxyketone (sum formula: C<sub>7</sub>H<sub>10</sub>O<sub>2</sub>) and acetone. According to quantum chemical calculations by Wang and Wang (2018), SABINOHBO2 can also undergo a unimolecular reaction with a rate coefficient of  $k \sim 5 \text{ s}^{-1}$  that eventually leads to the formation of a stable oxidation product with the sum formula C<sub>10</sub>H<sub>16</sub>O<sub>5</sub> containing two hydroperoxide groups. The predicted reaction rate coefficient makes this unimolecular reaction competitive with bimolecular reactions even  
100 in the presence of a high NO mixing ratio (~20 ppbv).

The primary alkyl radical from the addition of OH to the cyclic carbon (reaction path (a) in Fig. 1) forms a RO<sub>2</sub> radical SABINOHBO2, which mainly reacts with NO, HO<sub>2</sub>, and RO<sub>2</sub> in bimolecular reactions. Rate coefficients of unimolecular reactions are predicted to be too slow ( $k < 10^{-3} \text{ s}^{-1}$ ; Wang and Wang (2018)) to be competitive with bimolecular reactions. The reaction between SABINOHBO2 and NO forms eventually a HO<sub>2</sub> radical together with sabinaketone (sum formula: C<sub>9</sub>H<sub>14</sub>O).

105 Following the theoretical study by Wang and Wang (2017), the ozonolysis of sabinene results in the production of either sabinaketone together with formaldehyde oxide (CH<sub>2</sub>OO) with a yield of 17 % (reaction path (A) in Fig. 2) or formaldehyde (HCHO) together with either one of two types of Criegee intermediates (CI-1 with a yield of 45 % through reaction pathway (C), or CI-2 with a yield of 38 % through reaction pathway (B), Fig. 2). The respective yields are similar to the analogous pathways in the ozonolysis of β-pinene having yields of 5 % for CH<sub>2</sub>OO, and 46 % and 49 % for the analogous Criegee  
110 intermediates CI-1 and CI-2, respectively (Nguyen et al., 2009). In the atmosphere, formaldehyde oxide (CH<sub>2</sub>OO) reacts mainly with water to form formic acid and hydroxymethyl hydroperoxide (HMHP) (Long et al., 2016; Nguyen et al., 2016; Vereecken et al., 2017). The Criegee intermediate CI-2 also reacts mainly with water to form α-hydroxyalkyl hydroperoxide (AHAP, Fig. 2) under humid conditions, whereas in dry conditions a competitive unimolecular reaction leads to the formation of lactones. The α-hydroxyalkyl hydroperoxide can further decompose to sabinaketone in a reaction that is catalyzed by water  
115 and acids making the yield of sabinaketone depends on the water vapor concentration. This might explain the difference in the sabinaketone yield expected from the branching ratio of the ozonolysis pathway (A) of 17 % in the mechanism by Wang and Wang (2017) and yields between 35 % to 50 % observed in experiments performed in the presence of water vapor. (Hakola et al., 1994; Yu et al., 1999; Chiappini et al., 2006). The Criegee intermediate CI-1 exclusively undergoes a 1-4 H-shift reaction forming a vinyl hydroperoxide (VHP) that subsequently decomposes to an OH radical and a vinyloxy radical. The vinyloxy radical  
120 then reacts with O<sub>2</sub> forming a RO<sub>2</sub> radical (SABINO3O2), which is expected to further react in bimolecular reactions with NO, HO<sub>2</sub>, and other RO<sub>2</sub> radicals leading eventually to closed-shell oxidation products.

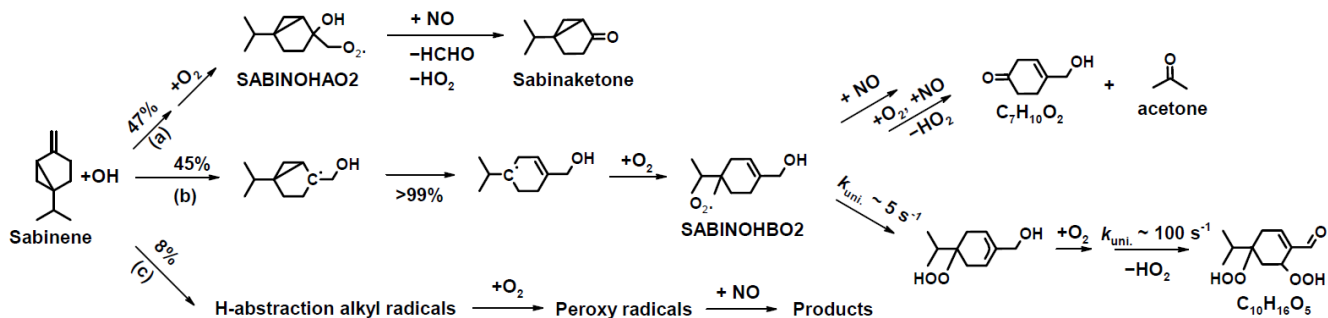


Figure 1. Simplified mechanism of the oxidation of sabinene by OH by Wang and Wang (2018). Only the pathways that are relevant for the experimental conditions in this study are shown.

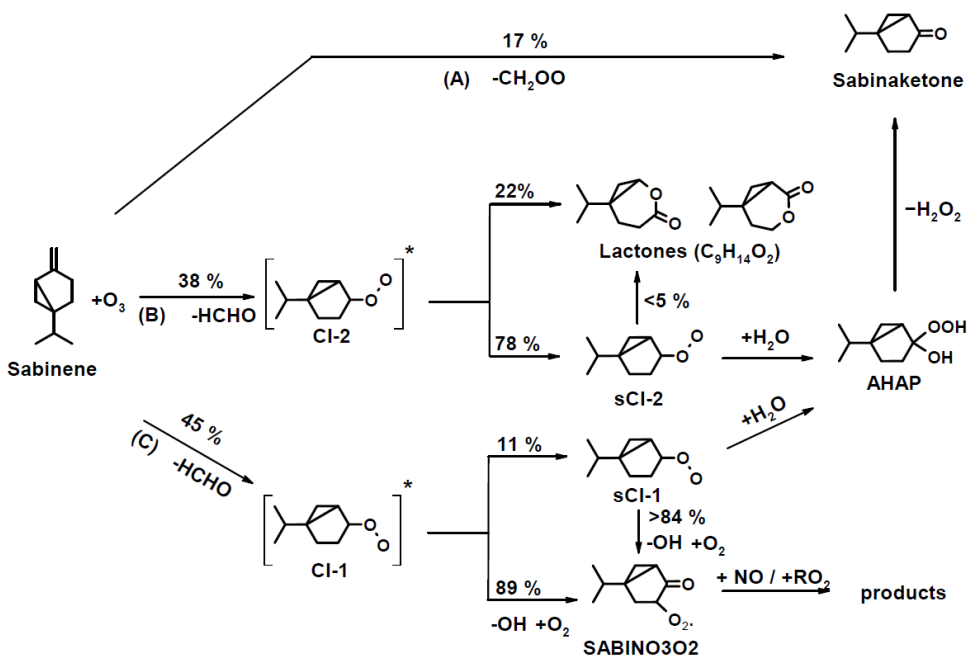


Figure 2. Simplified mechanism of the ozonolysis of sabinene by Wang and Wang (2017).

**3.1 Determination of the temperature-dependence of  $k_{\text{SAB+OH}}$  with OH reactivity measurements**

The rate coefficient of the reaction between sabinene and OH at temperatures between 284 K and 340 K was determined in the laboratory from OH reactivity ( $k_{\text{OH}}$ ) measurements using a laser flash-photolysis laser-induced fluorescence (LP-LIF) instrument (Lou et al., 2010; Fuchs et al., 2017). In a temperature-controlled flow tube, OH radicals are generated in situ by  
135 photolysis of  $\text{O}_3$  using laser pulses of a quadrupled Nd:YAG laser at a wavelength of 266 nm and a low pulse repetition rate of 1 Hz.  $\text{O}(^1\text{D})$  atoms produced from the photolysis of  $\text{O}_3$  react with water vapor present in the gas mixture to produce OH radicals. Air containing a well-known concentration of sabinene is continuously passed through the flow tube. Sabinene reacts with OH, which leads to the destruction of OH radicals. The decreasing OH radical concentration is detected via laser-induced fluorescence after excitation by short laser pulses (308 nm wavelength, 8.5 kHz pulse repetition frequency) in a low-pressure  
140 ( $\sim 4$  hPa) cell and monitored by single photon counting. A single exponential fit to the time series of the OH concentration directly gives the OH reactivity.

Gas mixtures of sabinene in synthetic air were prepared by injecting liquid sabinene (Roth Chemicals, GC grade, purity  $>98\%$ ) with a syringe in an evacuated SilcoNert coated canister (Restek, volume 6 L). The canister was subsequently pressurized to up to 3.5 bar with pure synthetic air prepared from ultrapure liquid nitrogen and oxygen (79 %  $\text{N}_2$ , 21 %  $\text{O}_2$ , Linde, purity  $>$   
145 99.9999 %), resulting in mixing ratios of about 6 ppmv sabinene. The concentration of sabinene in the canister was determined by measuring the total organic carbon (TOC) concentration using a catalytic oxidation at high temperature. In this method, a small flow (500 sccm) from the canister flowed through a pre-oven at 760 °C (1033 K) and afterward over a palladium catalyst at 500 °C (773 K). The concentration of carbon dioxide was measured by a cavity ring-down spectrometer (CRDS, Picarro). The catalytic conversion from VOCs to  $\text{CO}_2$  was tested with other VOCs (alkanes, aromatics and monoterpenes) and showed  
150 a complete conversion. Therefore, it can be assumed that sabinene was completely converted to  $\text{CO}_2$  during the TOC measurement. Assuming that all carbon stems from sabinene, its concentration in the canister can be calculated from the measured  $\text{CO}_2$  concentrations.

In the OH reactivity instrument, small flows (10 sccm) of sabinene and of synthetic air (100 sccm), to which  $\text{O}_3$  was added, were mixed into a high flow (20,000 sccm) of humidified synthetic air (water mixing ratio between 0.7 and 1.3 %) in the flow  
155 tube. The temperature of the flow tube was controlled by circulating water within a range of 10 °C to 70 °C (283 K to 343 K) and monitored with two PT100 temperature sensors. All flows were controlled by calibrated mass flow controllers. The sabinene mixing ratio in the flow was circa 5 ppbv. The  $\text{O}_3$  concentration in the flow tube was 22 ppbv measured by an  $\text{O}_3$  analyzer.

In total, three experiments were performed to measure the rate coefficients of the reaction of sabinene and OH ( $k_{\text{SAB+OH}}$ ) at  
160 seven different temperatures between 10 °C to 70 °C (283 K to 343 K). Two batches (A and B) of sabinene gas mixtures were measured, with batch A being measured twice. After reaching a stable temperature, the OH reactivity of the air without

sabinene (zero reactivity) was first measured for about 30 minutes, followed by the measurement of air with sabinene for another 40 minutes. The procedure was then repeated at different temperatures. The OH reactivity of air with sabinene was subtracted by its corresponding zero reactivity ranging from  $2 \text{ s}^{-1}$  to  $3 \text{ s}^{-1}$ . The rate coefficient of the OH reaction was calculated  
165 by using the sabinene concentration in the canister ( $[\text{SAB}]_0$ ) and the dilution factor  $f_{\text{dil}}$  determined from the flow rates:

$$k_{\text{SAB+OH}} = k_{\text{OH}} \cdot ([\text{SAB}]_0 \cdot f_{\text{dil}})^{-1} \quad (1)$$

The determination of the sabinene concentration in the canister with the TOC method is the predominant contributor to the uncertainty of the calculated reaction rate coefficients, resulting in uncertainties of about 2.5 % to 5.0 %. The loss of sabinene to  $\text{O}_3$  can be neglected (0.005 % at 293 K) due to the short residence time of less than two seconds in the flow tube.

The temperature dependence of the reaction rate coefficient  $k_{\text{SAB+OH}}$  can be expressed by the Arrhenius equation:

$$k_{\text{SAB+OH}}(T) = A \cdot \exp\left(-\frac{E_A}{R} \cdot \frac{1}{T}\right) \quad (2)$$

170 where  $A$  is a pre-exponential factor,  $E_A$  is the activation energy,  $T$  is the temperature and  $R$  is the universal gas constant. The temperature dependence coefficient  $-E_A/R$  is determined by a regression analysis of the reaction rate coefficient  $k_{\text{SAB+OH}}$  as a function of the inverse temperature.

### 3.2 Atmospheric simulation chamber SAPHIR

Sabinene oxidation experiments were performed in the atmospheric simulation chamber SAPHIR. A detailed description of  
175 the chamber can be found in previous publications (e.g., Rohrer et al., 2005; Kaminski et al., 2017). In brief, SAPHIR is a cylindrically shaped (5 m diameter, 18 m length) outdoor chamber with an inner volume of  $270 \text{ m}^3$  which is confined by a double-walled Teflon film (FEP) The high volume-to-surface ratio minimizes wall effects. A shutter system can be opened and closed for experiments to be performed in the dark (shutters closed) or in the sunlit (shutters opened) chamber. The entire spectrum of solar radiation is transmitted by the FEP film allowing for photooxidation experiments to be performed under  
180 natural conditions. The air pressure inside the SAPHIR chamber is kept slightly above atmospheric pressure (15 Pa) to ensure that air outside the chamber cannot leak into the chamber. The replenishment flow required to keep the overpressure results in the dilution of trace gases with a rate of approximately  $4 \text{ \% h}^{-1}$ . The temperature in the chamber is similar to the ambient temperature.

All experiments in this work were performed in synthetic air produced from evaporating ultrapure liquid oxygen and nitrogen  
185 (Linde, purity  $> 99.9999 \text{ \%}$ ). Before the start of the experiment, the chamber was flushed with synthetic air until trace gas concentrations were below the detection limit of the instruments. The air was then humidified by flushing water vapor from boiling Milli-Q water into the chamber together with a high flow of synthetic air. In the illuminated chamber, nitrous acid (HONO), NO, acetone, and HCHO are produced at a rate of several hundred pptv  $\text{hr}^{-1}$  presumably from chamber wall reactions

(Rohrer et al., 2005). Production rates were determined from the measured increase of their concentrations before sabinene  
190 was injected. The photolysis of HONO by sunlight is the major source of OH and NO in the experiments.

### 3.3 Instrumentation

Concentrations of trace gas ( $O_3$ , NO,  $NO_2$ , VOCs) and radical species (OH,  $HO_2$ ,  $RO_2$ ), photolysis frequencies (Bohn et al.,  
2005; Bohn and Zilken, 2005), and OH reactivity were measured in the chamber experiments in this work. The set of  
195 instruments used is listed in Table 1. Only the descriptions of measurements of species and quantity of interest (radicals, OH  
reactivity, and VOCs) in this study are included below.

OH concentrations were measured by two instruments making use of either differential optical absorption spectroscopy  
(DOAS) (Dorn et al., 1995) or laser-induced fluorescence (LIF) (Fuchs et al., 2011). The DOAS instrument measured the  
absorption of light at 308 nm produced by a pico-second dye laser system. The 2 km long absorption path was folded in a  
200 White cell along the long axis of the cylindrical-shaped chamber.

The LIF instrument consists of three measurement cells for the separate detection of OH,  $HO_2$ , and  $RO_2$  radicals. For the  
detection of OH, about  $1100 \text{ cm}^3 \text{ min}^{-1}$  of air is sampled into a low-pressure fluorescence cell (OH cell), in which OH radicals  
are excited by a short laser pulse at 308 nm. The subsequent fluorescence signal is measured by a single photon-counting  
system (Fuchs et al., 2011).

205  $HO_2$  radicals were indirectly detected in the  $HO_x$  cell, where  $HO_2$  radicals were first converted to OH radicals in the reaction  
with NO followed by the detection of OH with fluorescence. The concentration of NO is chosen, such that the formation of  
 $HO_2$  from the concurrent conversion of  $RO_2$  radicals is minimized (Fuchs et al., 2011). The OH-fluorescence signal measured  
in the  $HO_x$  cell represents the sum of the concentrations of  $HO_2$  and OH radicals of sampled air. The  $HO_2$  concentration can  
then be derived using the difference in fluorescence signals measured in the OH cell and the  $HO_x$  cell.  $RO_2$  concentrations  
210 were indirectly measured in the  $RO_x$  cell, where  $RO_x (=RO_2+HO_2+OH)$  radicals in the sampled air are first converted to  $HO_2$   
by adding NO and CO in a conversion reactor (Fuchs et al., 2011). The air is then partly sampled into another low-pressure  
LIF detection cell, where  $HO_2$  is converted to OH by excess NO followed by the measurement of OH by fluorescence.  
Similarly, the  $RO_2$  concentration is finally derived from the difference between the fluorescence signals obtained in the  $RO_x$   
and the  $HO_x$  cells.

215 In three of the experiments, both the LIF and DOAS instruments were available. In the two ozonolysis experiments on 24 and  
25 January 2022 (Table 5), mean OH concentrations measured by the DOAS and LIF instruments were both low at around 0  
to  $1 \times 10^6 \text{ cm}^{-3}$  (Fig. 3 and Fig. S1). The mean value of the difference between OH concentrations measured by the two  
instruments was about  $0.7 \times 10^6 \text{ cm}^{-3}$ . This is about the  $1\sigma$  precision of measurements of the DOAS instrument (Table 1). OH



concentrations measured by the LIF instrument were used for the analysis of the ozonolysis experiments due to the higher time resolution and precision compared to that by the DOAS instrument.

OH concentrations measured by the LIF instrument were about 27 % higher than OH concentrations measured by the DOAS instrument in the photooxidation experiment (05 July 2022), when OH concentrations were well-above the  $1\sigma$  precision of measurements. Differences were larger than the combined  $1\sigma$  accuracies of 15 % of the two instruments (7 % for the DOAS and 13 % for the LIF instruments). Because the DOAS instrument does not require calibration, its measurements are used for the analysis of the photooxidation experiments. The large difference might be due to an unaccounted calibration error of the LIF instrument.

OH radical concentrations were measured by only the DOAS instrument in the experiments on 06, 08 September 2021, 30 June 2022, and 05 July 2022. For the experiment on 06 July 2022, OH measurements were only available from the LIF instrument.

The OH reactivity in the chamber experiments was measured by a flash photolysis laser-induced fluorescence instrument as described in Section 3.1.

Sabinene was measured by proton-transfer-reaction mass spectrometry (Ionicon, PTR-TOF-MS). As the PTR-TOF-MS instrument was not calibrated for sabinene, the initial sabinene concentration right after the injection was determined by the increase in the measured OH reactivity using the rate coefficient  $k_{\text{SAB}+\text{OH}}$  (Section 4.1). The time series of the ion mass signal measured by the PTR-TOF-MS instrument was then scaled to match this initial sabinene concentration to derive the time series of sabinene concentrations.

Acetone was also measured and calibrated by the PTR-TOF-MS instrument. HCHO concentrations were measured by a CRDS instrument (Picarro) and by the DOAS instrument that also detected OH radicals. HCHO concentrations measured by the DOAS and the CRDS agreed within 20 % in two of the experiments. In the experiment on 30 June 2022 a discrepancy of 45 % was observed. DOAS measurements were used for the analysis on that day as the CRDS method requires correction factors, whereas the DOAS method directly gives concentration values (Glowania et al., 2021).

Sabinaketone, which is one of the major products expected to be formed from the oxidation of sabinene, was detected as an uncalibrated ion-mass signal by the PTR-TOF-MS instrument ( $m/z$ : 139). Here, the sensitivity of nopinone, an isomer of sabinaketone, for which the PTR-TOF-MS instrument was calibrated, is used to determine the sabinaketone concentration assuming that the instrument has the same sensitivity for both compounds. This assumption has an uncertainty of 50 % based on Sekimoto et al. (2017).

Table 1. Instrumentation for radical and trace-gas measurements in the chamber experiments.

Species	Method	Time resolution	1 $\sigma$ precision	1 $\sigma$ accuracy
OH	DOAS <sup>a</sup>	205 s	$0.8 \times 10^6 \text{ cm}^{-3}$	6.5 %
OH	LIF <sup>b</sup>	47 s	$0.3 \times 10^6 \text{ cm}^{-3}$	13 %
HO <sub>2</sub> , RO <sub>2</sub>	LIF	47 s	$1.5 \times 10^7 \text{ cm}^{-3}$	16 %
OH reactivity	Laser flash photolysis + LIF	180 s	0.3 s <sup>-1</sup>	0.5 s <sup>-1</sup>
NO	Chemiluminescence	60 s	20 pptv	5 %
NO <sub>2</sub>	Chemiluminescence + photolytic converter	60 s	20 pptv	5 %
O <sub>3</sub>	UV absorption	180 s	60 pptv	5 %
Sabinene	PTR-TOF-MS <sup>c</sup>	40 s	10 %	25 %
Sabinaketone	PTR-TOF-MS	40 s	10 %	50 %
HCHO	DOAS	100 s	20 %	7 %
HCHO	CRDS <sup>d</sup>	300 s	90 pptv	10 %
Acetone	PTR-TOF-MS	40 s	5 %	5 %
Photolysis frequencies	Spectroradiometer	60 s	10 %	18 %

<sup>a</sup> Differential optical absorption spectroscopy. <sup>b</sup> Laser-induced fluorescence. <sup>c</sup> Proton-transfer-reaction time-of-flight mass spectrometry. <sup>d</sup> Cavity ring-down spectroscopy.

### 3.4 Chamber experiments investigating the oxidation of sabinene

In total, seven experiments were performed to investigate the oxidation of sabinene by OH and O<sub>3</sub> under different conditions (Table 2). Two ozonolysis experiments were performed in winter 2022 at a low temperature of about 5 °C. In both experiments, the air was first humidified to a relative humidity of about 20 % (absolute humidity of 0.25 %). In the experiment on 24 January 2022 (Fig. 3, Novelli et al., 2023a), 6 ppbv of sabinene was injected followed by the addition of 100 ppbv O<sub>3</sub> 30 minutes after the sabinene injection. Sabinene was oxidized for 3.5 hours by O<sub>3</sub> and partly by OH radicals that were produced from the ozonolysis reaction. Then, 100 ppmv of CO was injected as OH scavenger followed by another injection of 8 ppbv sabinene 30 minutes later, so that sabinene nearly exclusively reacted with O<sub>3</sub> for another 3.5 hours. The experiment on 25 January 2022 (Fig. S1, Novelli et al., 2023b) was performed in a similar way as the experiment on 24 January 2022 except that about 240 ppbv of O<sub>3</sub> was injected at the beginning of the experiment and the total number of sabinene injections was four instead of two. RO<sub>2</sub> radicals were expected to react exclusively with HO<sub>2</sub> radicals in the absence of NO, if only bimolecular reactions of RO<sub>2</sub> radicals are considered. The self-reaction between RO<sub>2</sub> radicals is expected to be of minor importance compared to the reaction with HO<sub>2</sub> radicals, as the reaction rate constant of self-reactions of RO<sub>2</sub> is about 20 times slower than that of the reaction with HO<sub>2</sub> radicals (Supplementary material Section 1).

Five photooxidation experiments were performed in summer 2021 and 2022 (Table 2). In each experiment, the chamber air was first humidified to a relative humidity between 50 % and 70 % (absolute humidity of 1.0 % to 2.0 %). Before the injection of sabinene, the chamber roof was opened to allow sunlight to irradiate the chamber air. No OH reactant was added during this part of the experiment (zero-air phase) to determine the production rate of chamber sources for HONO, NO, acetone, and  
270 HCHO.

Thirty minutes to two hours after opening the chamber roof, between 3 ppbv and 5 ppbv of sabinene was injected into the chamber and re-injected two to three times after most of the sabinene had been oxidized. In the experiments on 30 June 2022 (Fig. S2, Novelli et al., 2023c) and 06 July 2022 (Fig. S3, Novelli et al., 2023d), 60 ppbv and 120 ppbv of O<sub>3</sub> was injected into the chamber before opening the roof, respectively, to reduce the NO mixing ratios to less than 0.5 ppbv (denoted as ‘low NO  
275 experiments’). In the experiments on 06 September 2021 (Fig. S4, Novelli et al., 2023e) and 05 July 2022 (Fig. 4, Novelli et al., 2023f), there was no O<sub>3</sub> addition (denoted as ‘medium NO experiments’), so that NO concentrations reached between 0.4 ppbv and 1.5 ppbv. The first part of the experiment on 08 September 2021 (Fig. S5, Novelli et al., 2023g) was like the other experiments with medium NO. In the second part of the experiment, however, 60 ppbv of O<sub>3</sub> was injected, such that NO mixing ratios were suppressed and sabinene reacted under similar conditions like in the experiments with low NO mixing ratios. In  
280 the experiments with medium NO mixing ratios, sabinene almost exclusively (> 90 %) reacted with OH. In the experiments with low NO mixing ratios, only about 60 % to 80 % of sabinene reacted with OH and the remaining part reacted with O<sub>3</sub>. Over 80 % of RO<sub>2</sub> radicals were expected to react with NO and the remaining part mostly reacted with HO<sub>2</sub> radicals in the photooxidation experiments, if only bimolecular reactions of RO<sub>2</sub> radicals are considered. For the experiment on 06 July 2022, only around 60 % RO<sub>2</sub> radicals reacted with NO at the beginning due to the low NO concentration caused by cloudy weather.

285

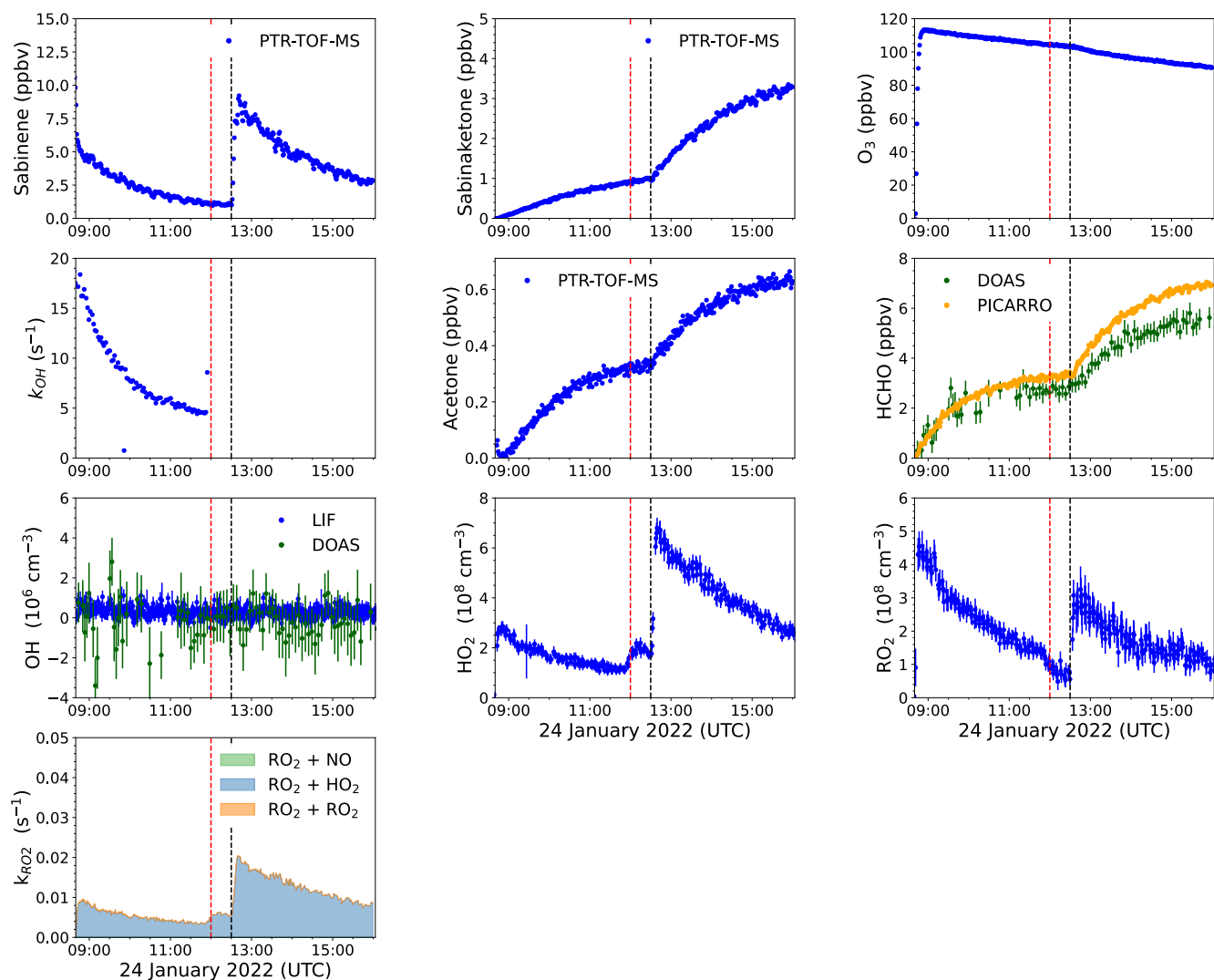


Figure 3. Overview plot of measured radical and trace gas concentrations in the ozonolysis experiment performed on 24 January 2022 (Novelli et al., 2023a). PTR-TOF-MS measurements of sabinene were derived from scaling the ion mass signal to the increase of the OH reactivity right after the injections. The contributions of different pathways to the total loss rate coefficient of RO<sub>2</sub> radicals,  $k_{RO_2}$ , are calculated from the reactivity of RO<sub>2</sub> radicals to bimolecular reactions using measured trace gas concentrations (Supplementary material Section 1). The black vertical dotted line indicates the time when sabinene was injected and the red vertical dotted line indicates the time when 100 ppmv of CO was injected. After the injection of CO, the OH reactivity was too high to be measured ( $\sim 500 \text{ s}^{-1}$ ).

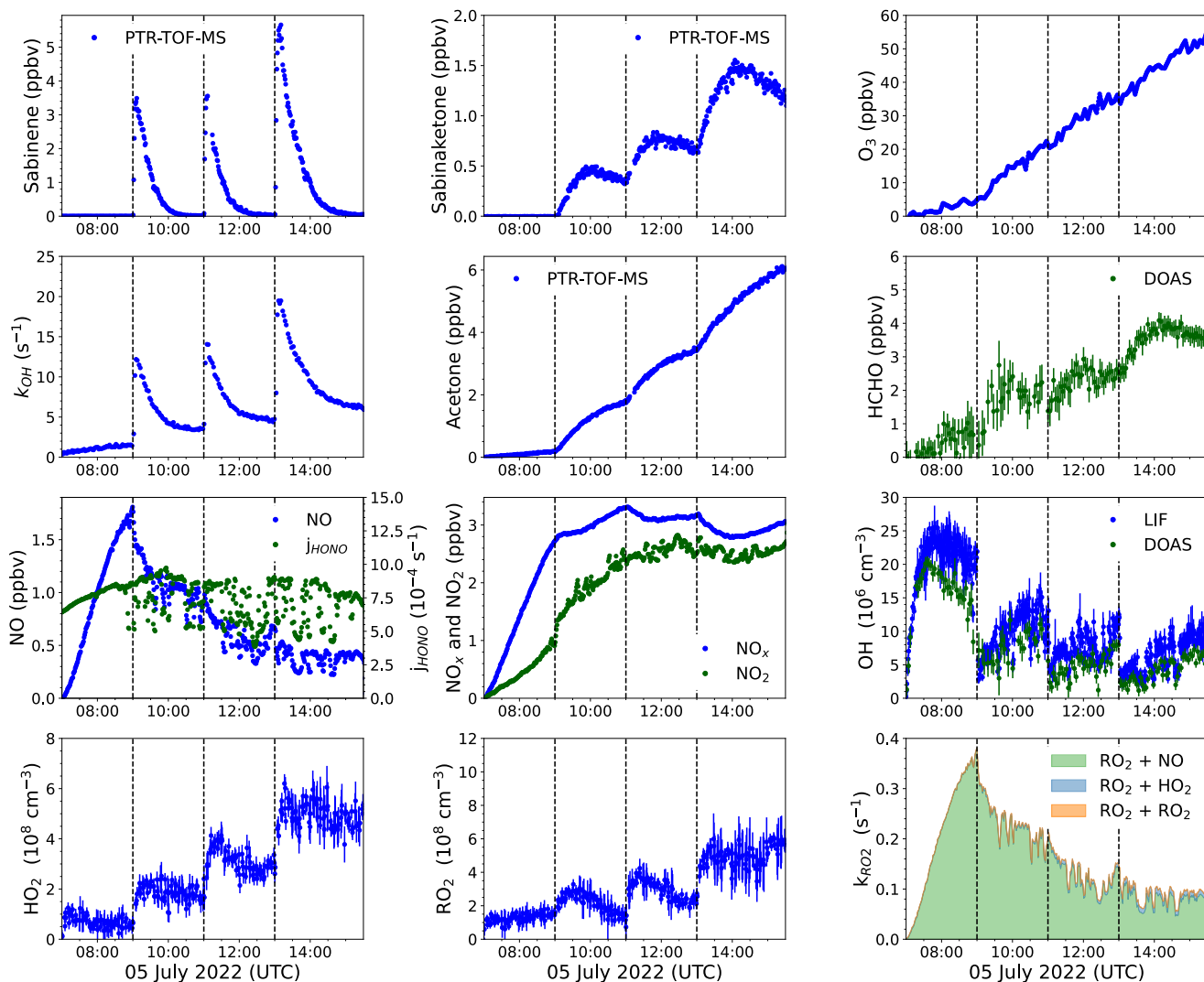


Figure 4. Overview plot of measured radical and trace gas concentrations in a photooxidation experiment with medium NO mixing ratios performed on 05 July 2022 (Novelli et al., 2023f). PTR-TOF-MS measurements of sabinene were derived from scaling the ion mass signal to the increase of the OH reactivity right after the injection. The contributions of different pathways to the total loss rate coefficient of RO<sub>2</sub> radicals,  $k_{RO_2}$ , are calculated from the reactivity of RO<sub>2</sub> radicals to bimolecular reactions using the measured trace gas concentrations (Supplementary material Section 1). Vertical dotted lines indicate times when sabinene was injected.

Table 2. Summary of conditions of experiments performed in this study. For temperature NO, OH, and O<sub>3</sub> concentrations, they are given as the range of mean values when sabinene was present in the chamber. The range of sabinene mixing ratios represents the range of maximum values reached right after each injection.

Type of experiment	Temperature (K)	NO (ppbv)	OH (10 <sup>6</sup> cm <sup>-3</sup> )	O <sub>3</sub> (ppbv)	Sabinene (ppbv)	Date	Figure	Reference
Ozonolysis	278 – 280	0	< 1	105	6	24 January 2022	Fig. 3	Novelli et al. (2023a)
	276 – 277	0	< 1	220	3 – 6	25 January 2022	Fig. S1	Novelli et al. (2023b)
Low NO	300 – 305	0.15 – 0.2	5 – 7	70 – 80	4 – 4.5	08 September 2021 (2 <sup>nd</sup> and 3 <sup>rd</sup> injections)	Fig. S5	Novelli et al. (2023g)
	299 – 307	0.2 – 0.3	3 – 4	60 – 75	4 – 8	30 June 2022	Fig. S2	Novelli et al. (2023c)
	293 – 297	0.05 – 0.15	2 – 5	100 – 110	4 – 6	06 July 2022	Fig. S3	Novelli et al. (2023d)
Medium NO	300 – 303	0.4 – 0.6	4 – 6	5 – 25	3.5	06 September 2021	Fig. S4	Novelli et al. (2023e)
	294 – 299	0.5	3 – 6	0 – 15	4	08 September 2021 (1 <sup>st</sup> injection)	Fig. S5	Novelli et al. (2023g)
	303 – 305	0.5 – 1.5	2 – 5	10 – 40	4 – 6	05 July 2022	Fig. 4	Novelli et al. (2023f)

### 310 3.5 Calculation of yields of oxidation products

Product yields from the oxidation of sabinene are calculated by performing a linear regression between the concentrations of product species and the amount of sabinene that was oxidized. The measured time series of product concentrations for acetone, HCHO, and sabinaketone were corrected for their additional production from the chamber and their loss due to dilution, photolysis and reaction with OH radicals as described in Kaminski et al. (2017) and Rolletter et al. (2019). Photolysis rates and dilution rates were measured and reaction rate coefficients with OH radicals for acetone and HCHO were retrieved from IUPAC recommendations (Atkinson et al., 2006). The reaction rate coefficient of the reaction of sabinaketone and OH radicals is taken from measurements by Alvarado et al. (1998) and Carrasco et al. (2007) giving a value of  $6 \times 10^{-12} \text{ cm}^3 \text{ s}^{-1}$ . The potential loss of sabinaketone by photolysis is estimated using photolysis rates of ketones calculated in the MCM model (Atkinson et al. 2006). The maximum photolysis rate loss constant for ketones during the experiments was  $3 \times 10^{-6} \text{ s}^{-1}$ , which would result in only a negligible loss of sabinaketone yield.

### 3.6 Calculation of the reaction rate coefficients and OH yield in the ozonolysis of sabinene in the chamber experiments

The rate coefficient of the ozonolysis reaction of sabinene ( $k_{\text{SAB}+\text{O}_3}$ ) and the OH yield ( $\gamma_{\text{SAB}}$ ) of this reaction were determined from the ozonolysis experiment. Sabinene was lost by its reactions with OH and  $\text{O}_3$ , and by dilution when no OH scavenger was present. The loss rate is described by the differential equation:

$$\frac{d[\text{SAB}]}{dt} = -[\text{SAB}](k_{\text{SAB}+\text{O}_3}[\text{O}_3] + k_{\text{SAB}+\text{OH}}[\text{OH}] + k_{\text{dil}}) \quad (3)$$

Solving the differential equation Eq. (3) yields the following expression:

$$\ln \frac{[\text{SAB}]_0}{[\text{SAB}]_t} = k_{\text{SAB}+\text{O}_3} \int_0^t [\text{O}_3]_{t'} dt' + k_{\text{SAB}+\text{OH}} \int_0^t [\text{OH}]_{t'} dt' + \int_0^t k_{\text{dil}} dt' \quad (4)$$

The reaction rate coefficient  $k_{\text{SAB}+\text{O}_3}$  is determined in the ozonolysis experiments in the presence of an OH scavenger, so that the sabinene loss in the reaction with OH becomes zero. The value of  $k_{\text{SAB}+\text{O}_3}$  can be obtained by rearranging Eq. (4).

$$k_{\text{SAB}+\text{O}_3} = \frac{\ln \frac{[\text{SAB}]_0}{[\text{SAB}]_t} - \int_0^t k_{\text{dil}} dt'}{\int_0^t [\text{O}_3]_{t'} dt'} \quad (5)$$

The uncertainty of the reaction rate coefficient  $k_{\text{SAB}+\text{O}_3}$  determined with this method is about 25 %, which is associated with the precision of the sabinene concentrations measurements (10 %), the accuracy of the  $\text{O}_3$  measurements (5 %, Table 1), and the choice of the time interval for the calculation. The error contributed by the accumulated dilution loss is insignificant as less than 5 % of sabinene was lost by dilution. The value of  $k_{\text{SAB}+\text{O}_3}$  in Eq. (5) depends on the time interval of integration. The integration starts at the time when the sabinene concentration reached its maximum for each injection of sabinene until the end of the experiment or the next sabinene injection, which is about 1 hour to 2 hours after the injections of sabinene. The value of rate coefficient  $k_{\text{SAB}+\text{O}_3}$  is then determined from the mean value of  $k_{\text{SAB}+\text{O}_3}$  calculated from every integration time step.

The calculation of the OH yield of the ozonolysis reaction is also based of Eq. (3). However, instead of integrating the loss of sabinene to OH and  $\text{O}_3$  for every time step within the time interval similar to the calculation of rate coefficient  $k_{\text{SAB}+\text{O}_3}$ , the calculation takes the average values of the dilution rate coefficient, OH and  $\text{O}_3$  concentrations:

$$\frac{d[\text{SAB}]}{dt} = -[\text{SAB}](t)(k_{\text{SAB}+\text{O}_3}\langle[\text{O}_3]\rangle_t + k_{\text{SAB}+\text{OH}}\langle[\text{OH}]\rangle_t + \langle k_{\text{dil}}\rangle_t) \quad (6)$$

$$\ln \left( \frac{[\text{SAB}]_0}{[\text{SAB}]_t} \right) + a = k_{\text{loss}} t = (k_{\text{SAB}+\text{O}_3}\langle[\text{O}_3]\rangle_t + k_{\text{SAB}+\text{OH}}\langle[\text{OH}]\rangle_t + \langle k_{\text{dil}}\rangle_t) t \quad (7)$$

where  $k_{\text{loss}}$  is the regression coefficient of the fitted exponential decay of the measured sabinene concentrations;  $a$  is the regression intercept. To determine the OH yield of the sabinene ozonolysis reaction  $\gamma_{\text{SAB}}$ , the OH concentration in Eq. (7) is expressed as a function of the OH production rate ( $P_{\text{OH}}$ ) and its loss rate. The loss rate of OH can be expressed as the product of OH reactivity  $k_{\text{OH}}$  and the OH concentration. Due to the short lifetime of the OH radical, the production rate of OH is always balanced by the destruction rate of OH. Here, it is assumed that OH radicals are only produced from the ozonolysis of sabinene

and the reaction of O<sub>3</sub> with HO<sub>2</sub> radicals. The OH reactivity can be assumed to be only from sabinene right after its injection  
 345 as contributions from species other than sabinene (O<sub>3</sub>, sabinaketone, HCHO, acetone etc.) to the total OH reactivity were less  
 than 10 % until half of the injected sabinene had reacted away. Therefore, only this time interval, which is about the first 30  
 minutes and 1 hour after the injection of sabinene, is used for this evaluation. Overall, the OH concentration can be expressed  
 as

$$[\text{OH}] = \frac{P_{\text{OH}}}{k_{\text{OH}}} \approx \frac{k_{\text{HO}_2+\text{O}_3}[\text{O}_3][\text{HO}_2] + k_{\text{SAB}+\text{O}_3}[\text{O}_3][\text{SAB}]\gamma_{\text{SAB}}}{k_{\text{SAB}+\text{OH}}[\text{SAB}]} \quad (8)$$

By combining Eq. (7) and Eq. (8), the total loss rate coefficient of sabinene  $k_{\text{loss}}$  without an OH scavenger, can be expressed  
 350 as a function of the reaction rate coefficient  $k_{\text{SAB}+\text{O}_3}$  and the OH yield  $\gamma_{\text{SAB}}$ , after correcting for the loss of sabinene to dilution  
 and the additional OH production from the reaction between HO<sub>2</sub> and O<sub>3</sub>.

$$k_{\text{loss, without CO}} = (k_{\text{SAB}+\text{O}_3}\langle[\text{O}_3]\rangle_t + k_{\text{SAB}+\text{OH}} \frac{k_{\text{HO}_2+\text{O}_3}[\text{O}_3][\text{HO}_2] + k_{\text{SAB}+\text{O}_3}[\text{O}_3][\text{SAB}]\gamma_{\text{SAB}}}{k_{\text{SAB}+\text{OH}}[\text{SAB}]} + \langle k_{\text{dil}} \rangle_t) \quad (9)$$

$$\frac{k_{\text{loss, without CO}} - \langle k_{\text{dil}} \rangle_t - \frac{k_{\text{HO}_2+\text{O}_3}\langle[\text{O}_3]\rangle_t\langle[\text{HO}_2]\rangle_t}{\langle[\text{SAB}]\rangle_t}}{\langle[\text{O}_3]\rangle_t} = k_{\text{SAB}+\text{O}_3}(1 + \gamma_{\text{SAB}}) \quad (10)$$

The value of rate coefficient  $k_{\text{SAB}+\text{O}_3}$  for the calculation of the OH yield is taken from the value calculated using Eq. (5). The  
 uncertainty of the OH yield  $\gamma_{\text{SAB}}$  can be as large as 50 % (Table S1). This is because the loss of sabinene by OH radicals is less  
 important than the loss of sabinene by the ozonolysis reaction and the uncertainty of the OH yield is enhanced by the  
 355 uncertainty of the ozonolysis reaction rate coefficient  $k_{\text{SAB}+\text{O}_3}$ . It is worth noting that potential systematic errors of about -20  
 % is not considered in the calculation, which arises from the assumption that the entire OH reactivity  $k_{\text{OH}}$  results from only  
 sabinene (Eq. (8)), and from the temperature difference of 2 °C to 4 °C between the ozonolysis experiments with and without  
 an OH scavenger. The value of the ozonolysis reaction rate coefficient  $k_{\text{SAB}+\text{O}_3}$  could be lower by 10 to 15 % at a temperature  
 of 276 K than at temperature of 280 K. This is estimated from the temperature dependence of ozonolysis rate constants of  
 360 structurally similar methylpropene and  $\beta$ -pinene, for which ozonolysis temperature-dependent reaction rate coefficients are  
 reported in Cox et al. (2020).

The usage of mean quantities ( $\langle[\text{OH}]\rangle_t$  and  $\langle[k_{\text{dil}}]\rangle_t$ ) to calculate the OH yield of the ozonolysis reaction can be justified, as the  
 time interval of the measurements that is used for the calculation of OH yield (30 minutes to 1 hour) is shorter than that of the  
 rate coefficient  $k_{\text{SAB}+\text{O}_3}$  (1 hour to 2 hours). The error arises from replacing O<sub>3</sub> concentrations with their mean values decreases  
 365 when a shorter time interval is considered. Using Eq. (7) to determine the OH yield by obtaining the regression coefficient  $k_{\text{loss}}$   
 is more robust than using Eq. (4) and calculates the OH yield for every timestep within the time interval of analysis, as  
 regression is less sensitive to the choice of reference sabinene concentration  $[\text{SAB}]_0$ .

The rate coefficient of the reaction of sabinene with OH  $k_{\text{SAB}+\text{OH}}$  was determined using measurements from the experiments  
 with medium NO mixing ratios (Table 2), because the contribution of the OH reaction to the total loss of sabinene was more  
 370 than 90 % in these experiments. The rate coefficient  $k_{\text{SAB}+\text{OH}}$  was determined by minimizing the root-mean-square error



between sabinene concentrations measured by the PTR-TOF-MS instrument and calculations using a simplified chemical model as described in Hantschke et al. (2021). The chemical model calculates the loss rate of sabinene with measured dilution rate, OH and O<sub>3</sub> concentrations with a time step of 1 minute. The simplified model only includes the chemical loss of sabinene by the reactions with OH and O<sub>3</sub> and by dilution, without other secondary chemistry. The rate coefficient of the ozonolysis reaction in the simplified model was taken from the recommended value ( $8.3 \times 10^{-17} \text{ cm}^3 \text{ s}^{-1}$ , Cox et al., 2020), as the temperature during the experiments in this study with medium NO mixing ratios was similar to that of the experiments reported in the literature, whereas the temperature in the ozonolysis experiment in this work was 20 °C lower. In the simulation, the OH concentration was constrained to measurements by either the DOAS or LIF instrument, depending on the availability of instruments. A value of the reaction rate coefficient  $k_{\text{SAB}+\text{OH}}$  was obtained for each injection of sabinene in the experiments with medium NO mixing ratios and each available OH instrument. The mean and standard deviation of the rate coefficient are then calculated with values from every injection obtained from an instrument.

### 3.7 Analysis of the chemical budget of OH radicals

Measurements in the chamber experiments were also used to study the chemical budget of OH radicals in the ozonolysis experiment and the photooxidation experiments at different NO mixing ratios. Since the lifetimes of OH is very short ( $< 1 \text{ s}$ ), the production rate of OH radical must equal its destruction rate on the time scale of the experiment. By considering radical production and destruction pathways that are typically included in atmospheric chemistry models, insights can be provided into if there are missing radical production pathways for example from fast RO<sub>2</sub>-isomerization reactions (e.g., Fuchs et al., 2013; Novelli et al., 2020), or if the rates of radical destruction pathways are underestimated (Pang et al., 2022). Table 3 lists all reactions producing OH radicals that were considered in the chemical budget analysis in this work. The destruction rate of OH radicals was calculated from the product of OH reactivity and OH concentration measurements (Hofzumahaus et al., 2009).

Table 3. Reactions producing OH radicals considered in the analysis of the chemical budget of radicals. Unless specified, reaction rate coefficients are given for room temperature ( $T = 298 \text{ K}$ ) and 1 atm pressure.

Reaction	$k$	$1\sigma$ uncertainty <sup>a</sup> (%)	Reference
$\text{HONO} + h\nu \rightarrow \text{OH} + \text{NO}$	$j_{\text{HONO}}$	35 <sup>b</sup>	Measured
$\text{O}_3 + h\nu + \text{H}_2\text{O} \rightarrow 2 \text{OH} + \text{O}_2$	$\phi_{\text{OH}}^c, j_{\text{O}_3}$	19	Measured
$\text{HO}_2 + \text{NO} \rightarrow \text{OH} + \text{NO}_2$	$8.8 \times 10^{-12} \text{ cm}^3 \text{ s}^{-1}$	20	Atkinson et al. (2004)
$\text{HO}_2 + \text{O}_3 \rightarrow \text{OH} + 2\text{O}_2$	$2.0 \times 10^{-15} \text{ cm}^3 \text{ s}^{-1}$	28	Atkinson et al. (2004)
sabinene + O <sub>3</sub> → 0.26OH + 0.26RO <sub>2</sub>	$8.3 \times 10^{-17} \text{ cm}^3 \text{ s}^{-1}$ (298 K)	16	Cox et al. (2020)
	$3.4 \times 10^{-17} \text{ cm}^3 \text{ s}^{-1}$ (278 K)	11	This study

395 <sup>a</sup>Total 1σ uncertainty of the reaction: including uncertainties from measurements, reaction rate coefficients and OH yield from ozonolysis. <sup>b</sup>HONO was not measured in all experiments, but its concentrations were calculated from OH, NO, and  $j_{\text{HONO}}$  measurements during the zero-air phase, the uncertainty in the HONO concentration is about 30 %. <sup>c</sup>yield of OH radicals of the photolysis of O<sub>3</sub>.

## 4. Results and Discussions

### 400 4.1 Rate coefficients of the reactions of sabinene with OH and O<sub>3</sub>

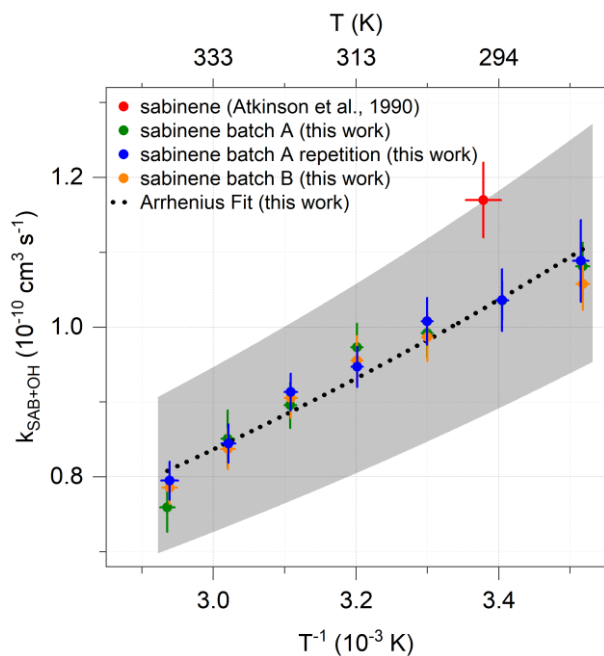
The average value of the ozonolysis reaction rate coefficient  $k_{\text{SAB}+\text{O}_3}$  determined from the chamber experiments in this work is  $(3.4\pm 0.8)\times 10^{-17}$  cm<sup>3</sup> s<sup>-1</sup> (Table S1). This value is 58 % lower than values reported in the literature (Table 4), in which the reaction rate coefficient  $k_{\text{SAB}+\text{O}_3}$  was determined at room temperature ((296±2) K) using absolute and relative rate techniques (Atkinson et al., 1990a, b; Bernard et al., 2012). The lower value determined in this study could be due to the low temperature  
405 (278 K) in the chamber experiments. This is supported by the known temperature dependence of ozonolysis rate coefficients of structurally similar alkenes such as isobutene, β-pinene, and camphene, for which values decrease by about 25 % to 50 % with relative uncertainties of about 25 % (Cox et al., 2020).

SAR in Jenkin et al. (2020) gives four to five times lower values for the ozonolysis reaction rate coefficient of sabinene than values determined in this work and reported in literature. Values are  $1.4\times 10^{-17}$  and  $9.3\times 10^{-18}$  cm<sup>3</sup> s<sup>-1</sup> at 298 K and 278 K,  
410 respectively. Since all experimentally determined values are higher, it is likely that SAR underpredicts the rate coefficient  $k_{\text{SAB}+\text{O}_3}$ . The large difference between the sabinene ozonolysis rate constants  $k_{\text{SAB}+\text{O}_3}$  determined experimentally and from the SAR developed by Jenkin et al. (2020) is likely related to the ring strain of the bicyclic ring. Species in that SAR with ozonolysis rate constants differing by more than a factor of three are mostly polycyclic compounds (e.g., camphene, α-copaene, and 3-carene) including sabinene. Since the SAR was constructed mostly with acyclic and monocyclic alkenes, it is likely that  
415 impacts of ring strain on the ozonolysis rate constant for polycyclic species cannot be properly captured.

The Arrhenius expression of the OH reaction rate coefficient  $k_{\text{SAB}+\text{OH}}$  derived from OH reactivity measurements at temperatures between 284 K and 340 K at ambient pressure in this work (Section 3.1) is

$$k_{\text{SAB}+\text{OH}}(T) = (1.67\pm 0.16)\times 10^{-11}\times \exp((537\pm 30)/T) \text{ cm}^3 \text{ s}^{-1}$$

The accuracy is 13 % to 15 % (Fig. 5), which is mainly due to the uncertainty of sabinene concentrations during the OH  
420 reactivity measurement. The value at room temperature (T = 298 K) is  $(1.0\pm 0.2)\times 10^{-10}$  cm<sup>3</sup> s<sup>-1</sup>. This agrees with the value required to describe the consumption of sabinene in the chamber experiments of  $(1.4\pm 0.5)\times 10^{-10}$  cm<sup>3</sup> s<sup>-1</sup> (Fig. S6), as well as the value of  $(1.17\pm 0.05)\times 10^{-10}$  cm<sup>3</sup> s<sup>-1</sup> determined in laboratory experiments Atkinson et al. (1990a). The temperature-dependence coefficient of the rate coefficient  $k_{\text{SAB}+\text{OH}}$  of (537±30) K is similar to that of structurally-similar β-pinene ((460±150) K) and isobutene ((505±200) K) (Mellouki et al., 2021).



425

Figure 5. The OH reaction rate coefficient  $k_{\text{SAB}+\text{OH}}$  determined in laboratory experiments using the OH reactivity measurements. The shaded area represents the accuracy of the Arrhenius expression.

Table 4. List of rate coefficients of the reaction of sabinene with OH and O<sub>3</sub> reported in literature and determined in this study.

	Reaction rate coefficient (cm <sup>3</sup> s <sup>-1</sup> )	Temperature (K)	Method	Reference
sabinene + OH	$(1.17 \pm 0.05) \times 10^{-10}$	296 ± 2	Relative rate	Atkinson et al. (1990a)
	$6.08 \times 10^{-11}$	298	SAR	Jenkin et al. (2018)
	$(1.67 \pm 0.16) \times 10^{-11} \times \exp((537 \pm 30)/T)$	284 – 340	OH reactivity measurements	This study
sabinene + O <sub>3</sub>	$(8.1 \pm 0.8) \times 10^{-17}$	296 ± 2	Absolute rate	Atkinson et al. (1990a)
	$(6.2 \pm 2.1) \times 10^{-17}$	297 ± 2	Absolute rate	Bernard et al. (2012)
	$(8.8 \pm 1.0) \times 10^{-17}$	296 ± 2	Relative rate	Atkinson et al. (1990b)
	$1.4 \times 10^{-17}$	298	SAR	Jenkin et al. (2020)
	$(3.4 \pm 0.8) \times 10^{-17}$	278 ± 2	Absolute rate	This work

430

## 4.2 Product yields of organic compounds from the oxidation of sabinene

Formaldehyde is one of the major products from the oxidation of sabinene by both oxidants, OH and O<sub>3</sub>. The analysis of the photooxidation experiments results in a HCHO yield of (46±25) %. The uncertainty is due to the uncertainty of the HCHO chamber source, corrections for the loss of HCHO, and the calculation of the amount of reacted sabinene. There is no significant difference in the HCHO yields determined in the experiments with either medium or low NO mixing ratios (Fig. 6a), which can be expected as the majority of RO<sub>2</sub> radicals reacted with NO in both experiments (Fig. S2 and Fig. 4). The HCHO yield reported in this study is higher than the yield of 25 % reported by Carrasco et al. (2006a) (Table 5), who conducted experiments at a high concentration (~ 2 ppmv) of sabinene using either H<sub>2</sub>O<sub>2</sub> or HONO photolysis as OH sources. The authors found similar HCHO yields in their experiments for different NO concentrations. Larsen et al. (2001) also performed experiments in the absence of NO and they a HCHO yield of (35±4) %. This value is lower than the yield found in this study but still agrees within uncertainties.

The photooxidation of sabinene results in an acetone yield of (21±15) % in this study (Fig. 6b), when OH radicals predominantly reacted with sabinene. The uncertainty of the acetone yield is mainly due to the uncertainty in the chamber source, corrections for losses, and the calculation of the amount of reacted sabinene. The value is consistent with the yields in the studies by Carrasco et al. (2006) and Reissell et al. (1999) (Table 5). Reissell et al. (1999) performed photooxidation experiments at high initial NO concentrations (~10 ppmv) and with a high NO:sabinene concentration ratio (~10:1). In another study by Larsen et al. (2001), the acetone yield was lower than the values found in this study and studies conducted by Reissell et al. (1999) and Carrasco et al. (2006).

The yield of sabinaketone of the photooxidation of sabinene is (18±16) % (Fig. 6c). The large uncertainty of the calculation is due to the uncertainty of the measurement sensitivity of sabinaketone. This value agrees well with literature values that range from 17 % to 24 % (Table 5). There is no significant dependence of the yield of sabinaketone from the OH oxidation of sabinene on the NO mixing ratio, which is also consistent with the findings in Carrasco et al. (2006).

The HCHO yield determined in the ozonolysis experiments is (48±15) %, when the OH oxidation was suppressed by the presence of an OH scavenger. This value is consistent with the yield of (52±9) % reported by Chiappini et al. (2006), who conducted ozonolysis experiments in the presence of an OH scavenger and with high concentrations (~ 1 ppmv) of sabinene and O<sub>3</sub>.

The ozonolysis of sabinene produces a small amount of acetone compared to the photooxidation by OH. The low acetone yield of (5±2) % determined in this study agrees well with those reported by Reissell et al. (1999) and Chiappini et al. (2006) (Table 5).

The yield of sabinaketone from the ozonolysis of sabinene is (31±15) %. This value is lower than values reported in literature, which range between 35 % to 50 %, but still agrees within the combined uncertainties (Hakola et al., 1994; Yu et al., 1999; Chiappini et al., 2006, Table 5). The sabinaketone yield could increase with increasing humidity due to the reaction of the

stabilized Criegee intermediates with water (Wang and Wang (2017), Fig. 2) and a laboratory study on the nopinone yield  
 465 from structurally-similar  $\beta$ -pinene ozonolysis (Ma and Marston, 2008). However, the absolute humidity during the ozonolysis  
 experiments in this study of 0.25 % was not much different or higher than the humidity in the experiments reported in literature  
 (Table 5), so it is unlikely that humidity explains the lower value in this work.

### 4.3 Production of OH radicals from sabinene ozonolysis

470 The OH yield from the sabinene ozonolysis reaction can be calculated by comparing the total loss rate coefficients of sabinene  
 in the presence and absence of an OH scavenger (Eq. (5) and (10), Table S1). An OH yield of (26 $\pm$ 29) % is obtained from the  
 experiments in this work. OH is not only produced from the ozonolysis reaction, but about 30 % to 40 % is produced from the  
 reaction of HO<sub>2</sub> with O<sub>3</sub> within the timeframe of the analyzed experiment. Productions of HO<sub>2</sub> radicals were observed once  
 sabinene started reacting with O<sub>3</sub>, which was likely related to the reaction between OH and O<sub>3</sub>, as well as the reactions of RO<sub>2</sub>  
 475 with other RO<sub>2</sub> radicals. The uncertainty of the OH yield is large, because the additional loss of sabinene from the reaction  
 with OH is small compared to the loss of sabinene from the ozonolysis reaction. The uncertainty of the ozonolysis rate  
 coefficient  $k_{\text{SAB}+\text{O}_3}$  further amplifies the uncertainty of the OH yield  $\gamma_{\text{SAB}}$  (Table S1).

The value determined in this work agrees with those reported in the literature of (26 $\pm$ 13) % (Atkinson et al., 1992) and  
 (33 $\pm$ 5) % (Aschmann et al., 2002). Calculating the OH yield  $\gamma_{\text{SAB}}$  without accounting for the contribution from HO<sub>2</sub>+O<sub>3</sub>, as in  
 480 previous studies due to the lack of HO<sub>2</sub> measurements, would result in a value of (41 $\pm$ 26) % for experiments in this work  
 (Table S1). This value is still in agreement with both literature values (Table 5).

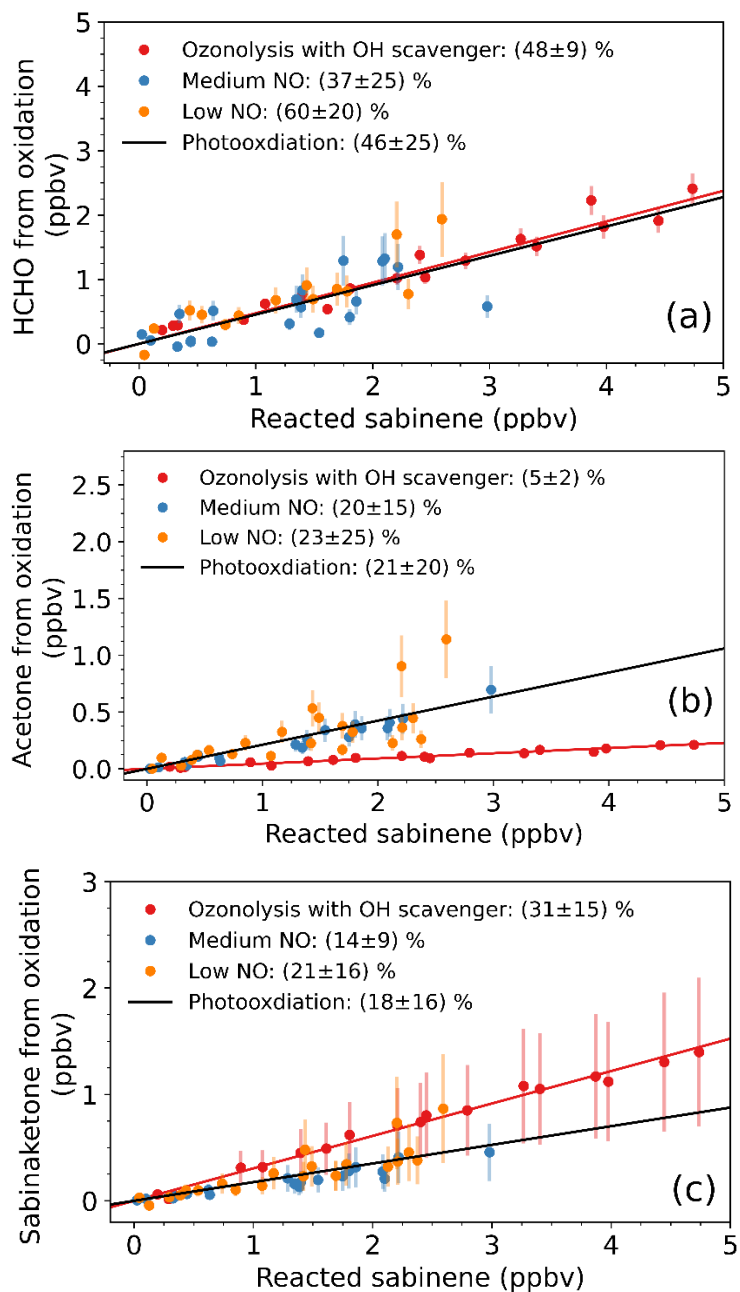
Table 5. Summary of the product yields from the oxidation of sabinene reported in literature and determined in experiments  
 in this study.

	Acetone	HCHO	Sabinaketone	OH	Reference
Sabinene + OH	/	/	17 %	NA	Arey et al. (1990)
	/	/	(17 $\pm$ 3) %	NA	Hakola et al. (1994)
	(19 $\pm$ 3) %	/	/	NA	Reissell et al. (1999)
	(9 $\pm$ 3) %	(35 $\pm$ 4) %	(24 $\pm$ 10) %	NA	Larsen et al. (2001)
	(25 $\pm$ 5) %	(25 $\pm$ 5) %	(22 $\pm$ 6) % (no NO <sub>x</sub> )	NA	Carrasco et al. (2006)
	(23 $\pm$ 5) %	(25 $\pm$ 6) %	(19 $\pm$ 5) % (with NO <sub>x</sub> )	NA	Carrasco et al. (2006)
	(21 $\pm$ 15) %	(46 $\pm$ 25) %	(18 $\pm$ 16) %	NA	This work
Sabinene + O <sub>3</sub>	(3 $\pm$ 2) %	/	/	/	Reissell et al. (1999)

/	/	(47±24) % <sup>a</sup>	/	Yu et al. (1999)
/	/	(50±9) % <sup>b</sup>	/	Hakola et al. (1994)
Detected	(52±9) %	(35±14) % <sup>c</sup>	/	Chiappini et al. (2006)
/	/	/	(33±5) %	Aschmann et al. (2002)
/	/	/	(26±13) %	Atkinson et al. (1992)
(5±2) %	(48±15) %	(31±15) % <sup>d</sup>	(26±29) %	This work

485 NA: Not applicable <sup>a</sup>Experiments were performed at around 5 % relative humidity (Griffin et al., 1999) <sup>b</sup>The humidity is not mentioned <sup>c</sup>Experiments were performed with less than 300 ppm of water <sup>d</sup>Ozonolysis experiments were conducted at 0.25 % absolute humidity.

490



495 Figure 6. Determination of the yields of HCHO (a), acetone (b), and sabinaketone (c) from the reaction of sabinene with OH and O<sub>3</sub>. ‘Photooxidation’ refers to the yields calculated from all data in the experiments with low and medium NO mixing ratios. For clarity, only data points from the time period, when 50 % of the injected sabinene was still present (3 ppbv to 4 ppbv) are shown. Fig. S7 shows the plots with the analysis using all data points.

#### 500 **4.4 Comparison of experimental results with values expected from the theoretically determined sabinene oxidation mechanism**

The product yields of the photooxidation of sabinene determined in this study can be compared to yields expected from the sabinene oxidation mechanisms by Wang and Wang (2017) and Wang and Wang (2018).

In the OH oxidation mechanism by Wang and Wang (2018), HCHO is only produced from the subsequent chemistry of the  
505 RO<sub>2</sub> radical SABINOHAO<sub>2</sub> that results from one of the two OH-addition reactions of sabinene (reaction pathway (a), Fig. 1). It is reasonable to expect that about 20 % to 35 % of RO<sub>2</sub> derived from the OH-oxidation of sabinene forms organic nitrates when it reacts with NO based on the study of peroxy radicals derived from monoterpenes oxidation (e.g., Rollins et al., 2010). Therefore, the HCHO expected from the OH-oxidation of sabinene should be 31 % to 38 % when considering the branching ratio of reaction pathway (a) stated in Wang and Wang (2018) and the organic nitrate yield. This agrees with the HCHO yield  
510 of (46±25) % (Table 5) determined in the photooxidation experiments.

The yield of acetone in the OH oxidation of sabinene expected from the mechanism by Wang and Wang (2018) is determined by the branching ratio of the OH-addition reaction producing the RO<sub>2</sub> radical SABINOHBO<sub>2</sub> as well as by the fraction of SABINOHBO<sub>2</sub> that undergoes an isomerization reaction or forms organic nitrates in the reaction with NO, from which eventually acetone is produced. For atmospheric conditions like in the experiments in this work, it is expected that more than  
515 90 % of SABINOHBO<sub>2</sub> undergoes the unimolecular reaction ( $k_{\text{uni}} \sim 5 \text{ s}^{-1}$ , Fig. 1) and less than 10 % undergoes bimolecular reactions ( $k_{\text{RO}_2} < 0.4 \text{ s}^{-1}$ , Fig. 4 and Figs. S2 and S3). Therefore, the acetone yield is expected to be only around 4 % (reaction path (b) in Fig. 1).

The experimentally determined acetone yield of (21±15) % is significantly higher than this value. To bring both values into agreement, the rate coefficient of the unimolecular reaction of SABINOHBO<sub>2</sub> would need to be in the same order as magnitude  
520 of the loss rates constant of bimolecular RO<sub>2</sub> reactions in this study ( $\sim 0.2 \text{ s}^{-1}$ ), so that about half of the RO<sub>2</sub> radical SABINOHBO<sub>2</sub> undergoes bimolecular reactions (mainly with NO). The uncertainty of the unimolecular reaction rate coefficient calculated in Wang and Wang (2018) of about  $5 \text{ s}^{-1}$  has an uncertainty of about one order of magnitude. Therefore, the unimolecular reaction rate constant calculated by Wang and Wang (2018) agrees with the rate constant required to reach a good agreement of acetone yield, despite the large difference between the acetone yield determined in the experiments and the  
525 yield expected from the mechanism in Wang and Wang (2018).

It should be noted that acetone might be produced from pathways other than the reaction pathways of RO<sub>2</sub> radical SABINOHBO<sub>2</sub> as suggested in Wang and Wang (2018). This would be consistent with the observation that the acetone yield found in this study and in Carrasco et al. (2006) does not strongly depend on the NO concentration (Table 5), which would be expected, if acetone is produced from reaction pathway without other competitions. For example, acetone might be produced  
530 from the bimolecular reactions of a RO<sub>2</sub> radical that does not have competing isomerization reactions, or could be produced



from a very fast isomerization reaction which bimolecular reactions cannot compete at typical NO concentrations in the atmosphere.

535 The sabinaketone yield of  $(18\pm 16)$  % from the OH-oxidation of sabinene determined from the experiment is lower than the yield of 31 % to 38 % expected from the mechanism by Wang and Wang (2018) after taking account into the branching ratio of reaction pathway (b) in Fig. 1 and the potential production of organic nitrates. The mechanism by Wang and Wang (2018) also suggests the production of sabinaketone comes together with the production of HCHO and thereby have the same yield. However, only the HCHO yield determined in this study agrees with the HCHO yield expected from the mechanism by Wang and Wang (2018). The large difference between the HCHO yield and sabinaketone yield in this study could be due to the large uncertainties of the yields.

540 Regarding the ozonolysis of sabinene, the HCHO yield determined in the experiments in this study and the study by Chiappini et al. (2006) are about 35 % lower than the HCHO yield of 83 % expected from the mechanism by Wang and Wang (2017). In their mechanism, HCHO is directly formed as co-product of the two Criegee intermediates CI-1 and CI-2, so that the HCHO yield reflects the sum of the branching ratios for these reaction pathways (reactions (B) and (C) in Fig. 2). The low HCHO yield in the experiments might therefore hint that the branching ratios in the mechanism by Wang and Wang (2017) are too  
545 high.

The production of acetone from the ozonolysis of sabinene is not discussed in Wang and Wang (2017). The small yield of  $(5\pm 2)$  % determined in this work also suggests that only minor reaction pathways lead to the production of acetone. One feasible mechanism could be the breakage of the 3-membered ring in the Criegee intermediate CI-2 that yields a biradical BI-RAD (Fig. 7). A similar mechanism was proposed for the Criegee intermediates from the ozonolysis of  $\beta$ -pinene (Nguyen et al., 2009). The expected yield of the analogous biradical formed from the ozonolysis of  $\beta$ -pinene is 3 %, which explains the low acetone yield between 1 % to 7 % observed for  $\beta$ -pinene (Lee et al., 2006). If a similar reaction pathway applies for Criegee intermediate from sabinene, it can be expected that this is mainly relevant for the Criegee intermediate CI-2 because of the fast loss of the Criegee intermediate CI-1 due to the fast H-migration reaction (Wang and Wang, 2017). Therefore, the small acetone yield might be explained by the breakage of the 3-membered ring of the Criegee intermediate CI-2.

555 The sabinaketone yield of  $(31\pm 15)$  % determined from the ozonolysis experiments is lower than the value of 47 % expected from the calculations by Wang and Wang (2017). As discussed above in the comparison with values reported in literature, humidity could impact the sabinaketone yield, but the overall effect is expected to be small. Values reported in literature are in better agreement with the yield of 47% expected from the mechanism by Wang and Wang (2017). Therefore, the low value determined in the work is likely due to the high uncertainty in the sabinaketone measurements.

560 The OH yield from the ozonolysis reaction of sabinene of  $(26\pm 29)$  % determined in the experiments is lower than the yield of 44 % expected from the mechanism in Wang and Wang (2017), but still within agreement due to the uncertainties presented in the experiment and the theoretical calculation. The OH yield expected from the mechanism is based on the fraction of

Criegee intermediate CI-1 that undergoes unimolecular decomposition forming an OH radical and an  $\beta$ -oxo alkyl radical (Fig. 2), which does not consider the potential OH production from Criegee intermediate  $\text{CH}_2\text{OO}$ . It is expected that about 40 % to 50 % of  $\text{CH}_2\text{OO}$  is stabilized by collision to form a stabilized Criegee intermediate and subsequently reacts with water at moderate humid conditions (Long et al., 2016; Nguyen et al., 2016; Pfeifle et al., 2018), and about 17 % of  $\text{CH}_2\text{OO}$  results in the production of an OH radical (Atkinson et al., 2006). Therefore, the additional contribution to the OH yield of the ozonolysis of sabinene from the chemistry of  $\text{CH}_2\text{OO}$  is only about 3 %.

Regarding the production of OH radicals from the chemistry of  $\text{C}_9$ -Criegee intermediates CI-1 and CI-2, the OH yield can be affected by the uncertainty of the yield of the stabilized Criegee intermediate sCI-1. Laboratory experiments quantifying the yield of the stabilized Criegee intermediate would partly help constraining the OH yield. However, to the best of our knowledge, there are no measurements of stabilized Criegee intermediates from the ozonolysis of sabinene.

The OH yield can also be affected by reaction mechanisms that were not investigated by Wang and Wang (2017). For example, OH radical may not form during the dissociation of vinyl hydroperoxide. The OH radical could reorientate and then recombine with the  $\beta$ -oxo alkyl radical, which could result in the production of 2-hydroxyketone (Barber et al., 2018; Kuwata et al., 2018, Fig. 8). With this additional mechanism, the theoretical OH yield of the ozonolysis of sabinene can be reduced. Though further investigation on the relative importance of the recombination pathway to the dissociation pathway is needed.

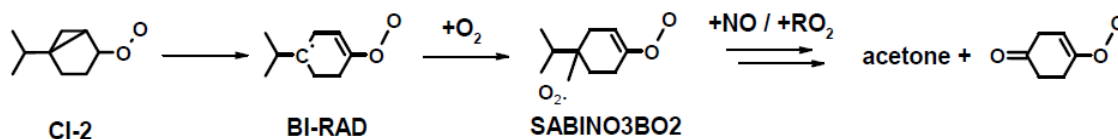


Figure 7. Possible reaction pathway of the Criegee intermediate CI-2 that could explain the small production of acetone from the ozonolysis of sabinene.

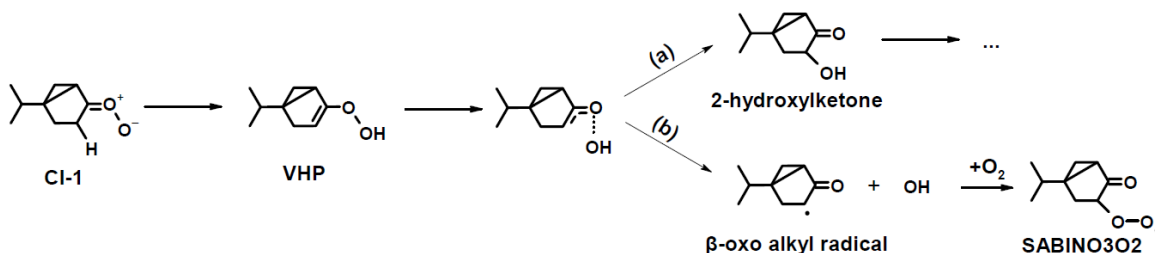


Figure 8. Possible pathways of the dissociation of vinyl hydroperoxide (VHP) from CI-1 that lead to the production of (a) 2-hydroxyketone, and (b) an OH radical and  $\beta$ -oxo alkyl radical.

#### 4.5 Chemical budget of OH radicals

The sum of OH radical production rates from different pathways needs to be balanced by the OH destruction rate. In the ozonolysis experiment (Fig. 9a), the production and destruction rates of OH were low with values of less than 1.5 ppbv h<sup>-1</sup>. The OH concentration was close to the limit of detection of the instrument ( $< 10^6 \text{ cm}^{-3}$ ), so that the calculations have a high uncertainty. In the first hour of the experiment, about 65 % of the total OH production was from the ozonolysis reaction (0.75 ppbv h<sup>-1</sup>) and the remaining part was from the reaction of HO<sub>2</sub> with O<sub>3</sub> (0.5 ppbv h<sup>-1</sup>). The total production rate of OH was on average slightly higher (+0.2 ppbv h<sup>-1</sup>) than the destruction rate. However, this discrepancy is within the uncertainty of the calculations, so that the chemical budget can be regarded as balanced by the considered OH production and destruction reactions.

595 In the photooxidation experiment with low NO mixing ratios (Fig. 9b), the production rate of OH ranged between 2 and 6 ppbv h<sup>-1</sup>. A good agreement between the OH production and destruction rates can be seen during the zero-phase demonstrating that the analysis includes all important OH production pathways in the clean chamber before sabinene was injected.

After the injection of sabinene, the OH destruction rate increased due to the consumption by sabinene. The OH production rate concurrently increased due to the enhanced regeneration of OH from the reaction of HO<sub>2</sub> with NO and due to the production of OH from the ozonolysis of sabinene. For NO mixing ratios (0.05 ppbv to 0.15 ppbv) in this experiment, 20 % to 60 % of the OH was produced from OH regeneration in the reaction of HO<sub>2</sub> with NO, and the remaining part was from the photolysis of HONO and O<sub>3</sub> and the reaction of HO<sub>2</sub> with O<sub>3</sub>. The contribution of the ozonolysis of sabinene to the total OH production was maximum 10 % to 30 % right after both sabinene injections, but quickly decreased, while sabinene was being oxidized. Overall, the OH production rate was very well balanced by the OH destruction rate in the experiments with low NO mixing ratios suggesting that there was no significant missing OH sources for the conditions of these experiments.

605 In the photooxidation experiment with medium NO concentrations (Fig. 9c), the OH production and destruction rates were 4 ppbv to 10 ppbv h<sup>-1</sup> which was higher than values in the experiments with low NO. The high production rate is mainly due to a fast regeneration of OH in the reaction of HO<sub>2</sub> with NO contributing 70 % to 80 % to the total OH production rate. The production rate of OH was also well balanced by the OH destruction rate within the uncertainty of the calculations in this experiment.

In summary, the OH production and destruction rates were well-balanced for all conditions experienced in this work. This suggests that there are no unaccounted OH production reactions in the photooxidation of sabinene, so that well-known photolysis reactions and bimolecular reactions are sufficient to be considered in the chemical budget of OH radicals. This is consistent with the mechanism proposed by Wang and Wang (2018).

615

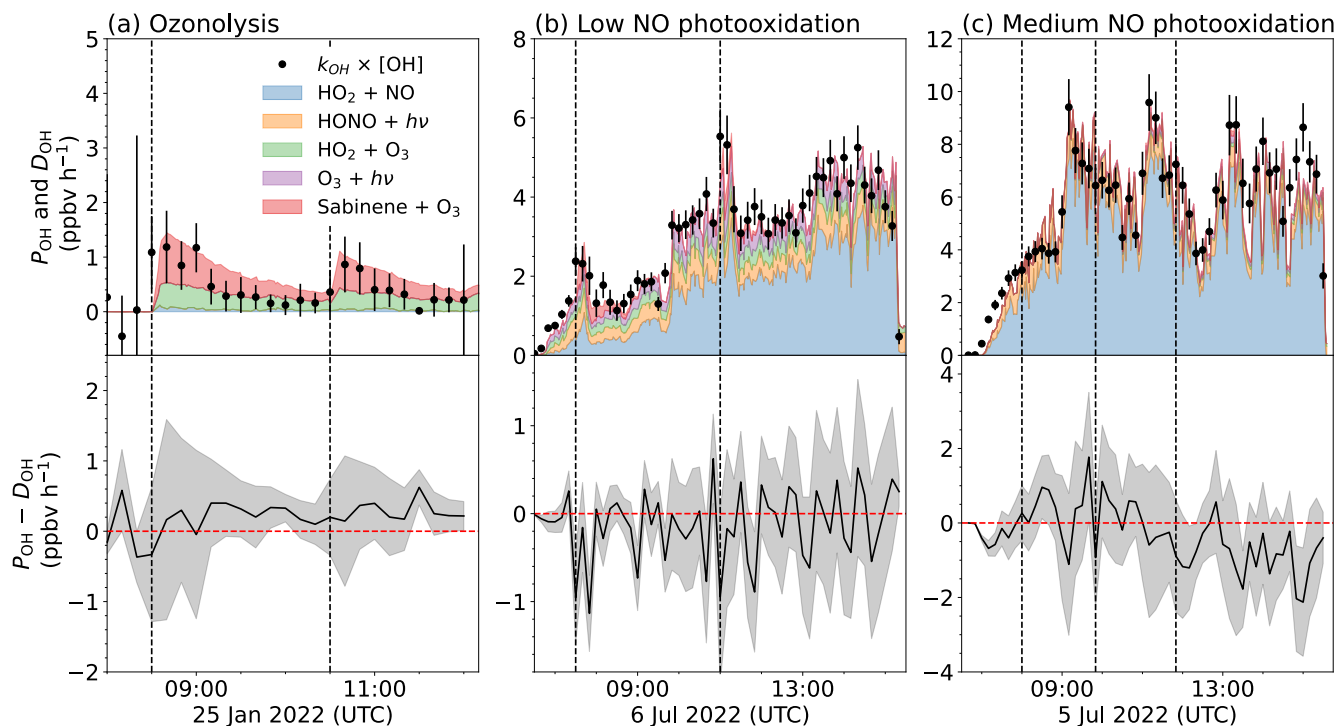


Figure 9. Overview of the production rate of OH ( $P_{OH}$ , coloured areas) and the destruction rate of OH ( $D_{OH}$ , black dots) (top panel), as well as their differences (bottom panel) in (a) an ozonolysis experiment, (b) experiments with low NO, and (c) with medium NO mixing ratios. Gray shaded areas are the  $1\sigma$  uncertainty of the difference between  $P_{OH}$  and  $D_{OH}$ .

620

## 5 Conclusions

The oxidation of sabinene by OH and  $O_3$  was investigated at different levels of NO ranging from zero to 2 ppbv in experiments conducted in the atmospheric simulation chamber SAPHIR. The experiments were performed at sabinene mixing ratios of 3 ppbv to 8 ppbv with  $O_3$  mixing ratios ranging from zero to 200 ppbv.

625 In addition to the chamber experiments, the Arrhenius expression of the rate coefficient of the oxidation of sabinene by OH radicals,  $k_{SAB+OH}$ , was determined from measurements using an OH reactivity instrument for temperatures ranging from 284 K to 340 K, giving  $(1.67 \pm 0.15) \times 10^{-11} \times \exp((537 \pm 30)/T) \text{ cm}^3 \text{ s}^{-1}$ . This agrees with the value determined in the chamber experiments at room temperature and the experimental value reported by Atkinson et al. (1990) within the uncertainties. The temperature-dependence coefficient of the Arrhenius expression of the rate coefficient  $k_{SAB+OH}$  is similar to those of the OH-oxidation of structurally-similar  $\beta$ -pinene and isobutene within uncertainties (Mellouki et al., 2021). The ozonolysis reaction

630

rate coefficient ( $k_{\text{SAB}+\text{O}_3}$ ) determined in the chamber experiment at 278 K is  $(3.4\pm 0.8)\times 10^{-17}$  cm<sup>3</sup> s<sup>-1</sup>, which is 58 % lower than the value determined in Atkinson et al. (1990) at 298 K.

635 Yields of oxidation products from the reaction of sabinene with OH and O<sub>3</sub> including HCHO, acetone, and sabinaketone were quantified in the chamber experiments. All yields determined in this study agree with yields reported in previous laboratory studies (e.g., Reissell et al., 1999; Aschmann et al., 2002; Carrasco et al., 2006; Chiappini et al., 2006).

The product yields calculated from the experiments in this study are compared to that expected from the mechanism proposed by Wang and Wang (2018). For the oxidation of sabinene by OH, the HCHO yield confirms branching ratios of the OH-addition reaction forming the RO<sub>2</sub> radical SABINOHAO<sub>2</sub>, but the sabinaketone yield is lower than that branching ratio.

640 The experimental acetone yield is 15 % absolute higher than the value expected from the mechanism, which could be explained by a fast isomerization reaction of the RO<sub>2</sub> radical SABINOHBO<sub>2</sub> in the mechanism outcompeting its bimolecular reaction with NO that produces acetone. The experimental acetone yields under NO mixing ratios between 0.1 ppbv to 0.5 ppbv are similar. These findings suggest that the isomerization rate coefficient of the RO<sub>2</sub> radical SABINOHBO<sub>2</sub> is slower than what was calculated by Wang and Wang (2018), or that the production of acetone is not affected by the competition between the isomerization reaction and the bimolecular reaction with NO.

645 Regarding the product from the ozonolysis of sabinene, HCHO, sabinaketone and OH yields determined from the experiments in this work are all lower than expected from the mechanism by Wang and Wang (2017). Further experiments are required to investigate the reason for these discrepancies, though the observed differences could be explained by the large uncertainties in the measurements.

650 The destruction rates of OH are in excellent agreement with the production rates of OH without considering additional production from for example potential isomerization reactions of RO<sub>2</sub> radical derived from the oxidation of sabinene. This is consistent with the proposed mechanism from Wang and Wang (2017), who calculated that there is no significant OH production from isomerization reactions of RO<sub>2</sub> in the oxidation mechanism of sabinene.

Data availability. Data from the experiments in the SAPHIR chamber used in this work are available on the EUROCHAMP data home page: <https://doi.org/10.25326/W4QV-KY95> (Novelli et al., 2023a); <https://doi.org/10.25326/8BA6-MM58> (Novelli et al., 2023b); <https://doi.org/10.25326/QDQE-8Q79> (Novelli et al., 2023c); <https://doi.org/10.25326/25V8-PA77> (Novelli et al., 2023d); <https://doi.org/10.25326/FCYS-Y288> (Novelli et al., 2023e); <https://doi.org/10.25326/B5VV-K378> (Novelli et al., 2023f); <https://doi.org/10.25326/BQVM-QR53> (Novelli et al., 2023g).

660 *Author contributions.*

JYSP, FB, PTMC, and HF wrote the manuscript; JYSP, PTMC, and HF designed and led the chamber experiments; FB, GG, and RD set up and conducted the measurement of OH reactivity and reaction rate coefficient in the laboratory. BB (radiation), MF and AN (radicals and OH reactivity), PTMC (formaldehyde and OH radicals), SW and GG (organic compounds), FR (nitrogen oxides and ozone) were responsible for the measurements of chamber experiments.

665 All the co-authors commented on and discussed the manuscript and contributed to the writing of the manuscript.

*Competing interests.* The authors declare to have no competing interests.

*Financial support.* This project has received funding from the European Research Council (ERC) under the European Union's Horizon 2020 research and innovation programme (SARLEP grant agreement No. 681529) and from the European Commission (EC) under the European Union's Horizon 2020 research and innovation programme (Eurochamp 2020 grant agreement No. 730997).

670

## References

- 675 Almatarneh, M. H., Elayan, I. A., Altarawneh, M., and Hollett, J. W.: A computational study of the ozonolysis of sabinene, *Theor. Chem. Acc.*, 138, 30, <https://doi.org/10.1007/s00214-019-2420-7>, 2019.
- Alvarado, A., Arey, J., and Atkinson, R.: Kinetics of the Gas-Phase Reactions of OH and NO<sub>3</sub> Radicals and O<sub>3</sub> with the Monoterpene Reaction Products Pinonaldehyde, Caronaldehyde, and Sabinaketone, *J. Atmos. Chem.*, 31, 281–297, <https://doi.org/10.1023/A:1006010915971>, 1998.
- 680 Arey, J., Atkinson, R., and Aschmann, S. M.: Product study of the gas-phase reactions of monoterpenes with the OH radical in the presence of NO<sub>x</sub>, *Journal of Geophysical Research: Atmospheres*, 95, 18539–18546, <https://doi.org/10.1029/JD095iD11p18539>, 1990.
- Aschmann, S. M., Arey, J., and Atkinson, R.: OH radical formation from the gas-phase reactions of O<sub>3</sub> with a series of terpenes, *Atmos. Environ.*, 36, 4347–4355, [https://doi.org/10.1016/S1352-2310\(02\)00355-2](https://doi.org/10.1016/S1352-2310(02)00355-2), 2002.
- 685 Atkinson, R. and Arey, J.: Gas-phase tropospheric chemistry of biogenic volatile organic compounds: a review, *Atmos. Environ.*, 37, 197–219, [https://doi.org/10.1016/S1352-2310\(03\)00391-1](https://doi.org/10.1016/S1352-2310(03)00391-1), 2003.
- Atkinson, R., Hasegawa, D., and Aschmann, S. M.: Rate constants for the gas-phase reactions of O<sub>3</sub> with a series of monoterpenes and related compounds at 296 ± 2 K: GAS-PHASE REACTIONS OF O<sub>3</sub>, *Int. J. Chem. Kinet.*, 22, 871–887, <https://doi.org/10.1002/kin.550220807>, 1990a.

- 690 Atkinson, R., Aschmann, S. M., and Arey, J.: Rate constants for the gas-phase reactions of OH and NO<sub>3</sub> radicals and O<sub>3</sub> with sabinene and camphene at 296±2 K, *Atmos. Environ.*, 24, 2647–2654, [https://doi.org/10.1016/0960-1686\(90\)90144-C](https://doi.org/10.1016/0960-1686(90)90144-C), 1990b.
- Atkinson, R., Aschmann, S. M., Arey, J., and Shorees, B.: Formation of OH radicals in the gas phase reactions of O<sub>3</sub> with a series of terpenes, *J. Geophys. Res.*, 97, 6065, <https://doi.org/10.1029/92JD00062>, 1992.
- 695 Atkinson, R., Baulch, D. L., Cox, R. A., Crowley, J. N., Hampson, R. F., Hynes, R. G., Jenkin, M. E., Rossi, M. J., and Troe, J.: Evaluated kinetic and photochemical data for atmospheric chemistry: Volume I - gas phase reactions of O<sub>x</sub>, HO<sub>x</sub>, NO<sub>x</sub> and SO<sub>x</sub> species, *Atmos. Chem. Phys.*, 4, 1461–1738, <https://doi.org/10.5194/acp-4-1461-2004>, 2004.
- Atkinson, R., Baulch, D. L., Cox, R. A., Crowley, J. N., Hampson, R. F., Hynes, R. G., Jenkin, M. E., Rossi, M. J., Troe, J., and IUPAC Subcommittee: Evaluated kinetic and photochemical data for atmospheric chemistry: Volume II – gas phase reactions of organic species, *Atmos. Chem. Phys.*, 6, 3625–4055, <https://doi.org/10.5194/acp-6-3625-2006>, 2006.
- 700 Barber, V. P., Pandit, S., Green, A. M., Trongsiwat, N., Walsh, P. J., Klippenstein, S. J., and Lester, M. I.: Four-Carbon Criegee Intermediate from Isoprene Ozonolysis: Methyl Vinyl Ketone Oxide Synthesis, Infrared Spectrum, and OH Production, *J. Am. Chem. Soc.*, 140, 10866–10880, <https://doi.org/10.1021/jacs.8b06010>, 2018.
- 705 Bernard, F., Fedioun, I., Peyroux, F., Quilgars, A., Daële, V., and Mellouki, A.: Thresholds of secondary organic aerosol formation by ozonolysis of monoterpenes measured in a laminar flow aerosol reactor, *J. Aerosol Sci.*, 43, 14–30, <https://doi.org/10.1016/j.jaerosci.2011.08.005>, 2012.
- Bohn, B. and Zilken, H.: Model-aided radiometric determination of photolysis frequencies in a sunlit atmosphere simulation chamber, *Atmos. Chem. Phys.*, 5, 191–206, <https://doi.org/10.5194/acp-5-191-2005>, 2005.
- 710 Bohn, B., Rohrer, F., Brauers, T., and Wahner, A.: Actinometric measurements of NO<sub>2</sub> photolysis frequencies in the atmosphere simulation chamber SAPHIR, *Atmos. Chem. Phys.*, 5, 493–503, <https://doi.org/10.5194/acp-5-493-2005>, 2005.
- Carrasco, N., Rayez, M. T., Rayez, J. C., and Doussin, J. F.: Experimental and theoretical study of the reaction of OH radical with sabinene, *Phys. Chem. Chem. Phys.*, 8, 3211, <https://doi.org/10.1039/b604489a>, 2006.
- 715 Carrasco, N., Picquet-Varrault, B., and Doussin, J.-F.: Kinetic and product study of the gas-phase reaction of sabinaketone with OH radical, *Int. J. Chem. Kinet.*, 39, 415–421, <https://doi.org/10.1002/kin.20252>, 2007.
- Chiappini, L., Carrasco, N., Temine, B., Picquet-Varrault, B., Durand-Jolibois, R., Wenger, J. C., and Doussin, J.-F.: Gaseous and Particulate Products from the Atmospheric Ozonolysis of a Biogenic Hydrocarbon, Sabinene, *Environ. Chem.*, 3, 286, <https://doi.org/10.1071/EN06037>, 2006.
- 720 Cox, R. A., Ammann, M., Crowley, J. N., Herrmann, H., Jenkin, M. E., McNeill, V. F., Mellouki, A., Troe, J., and Wallington, T. J.: Evaluated kinetic and photochemical data for atmospheric chemistry: Volume VII – Criegee intermediates, *Atmos. Chem. Phys.*, 20, 13497–13519, <https://doi.org/10.5194/acp-20-13497-2020>, 2020.

- Crouse, J. D., Paulot, F., Kjaergaard, H. G., and Wennberg, P. O.: Peroxy radical isomerization in the oxidation of isoprene, *Phys. Chem. Chem. Phys.*, 13, 13607–13613, <https://doi.org/10.1039/C1CP21330J>, 2011.
- 725
- Crouse, J. D., Knap, H. C., Ørnsø, K. B., Jørgensen, S., Paulot, F., Kjaergaard, H. G., and Wennberg, P. O.: Atmospheric Fate of Methacrolein. 1. Peroxy Radical Isomerization Following Addition of OH and O<sub>2</sub>, *J. Phys. Chem. A*, 116, 5756–5762, <https://doi.org/10.1021/jp211560u>, 2012.
- Dorn, H.-P., Neuroth, R., and Hofzumahaus, A.: Investigation of OH absorption cross sections of rotational transitions in the  $A^2\Sigma^+$ ,  $v'=0 \leftarrow X^2\Pi$ ,  $v''=0$  band under atmospheric conditions: Implications for tropospheric long-path absorption measurements, *J. Geophys. Res. Atmos.*, 100, 7397–7409, <https://doi.org/10.1029/94JD03323>, 1995.
- 730
- Fuchs, H., Bohn, B., Hofzumahaus, A., Holland, F., Lu, K. D., Nehr, S., Rohrer, F., and Wahner, A.: Detection of HO<sub>2</sub> by laser-induced fluorescence: calibration and interferences from RO<sub>2</sub> radicals, *Atmos. Meas. Tech.*, 4, 1209–1225, <https://doi.org/10.5194/amt-4-1209-2011>, 2011.
- 735
- Fuchs, H., Hofzumahaus, A., Rohrer, F., Bohn, B., Brauers, T., Dorn, H.-P., Häsel, R., Holland, F., Kaminski, M., Li, X., Lu, K., Nehr, S., Tillmann, R., Wegener, R., and Wahner, A.: Experimental evidence for efficient hydroxyl radical regeneration in isoprene oxidation, *Nat. Geosci.*, 6, 1023–1026, <https://doi.org/10.1038/ngeo1964>, 2013.
- 740
- Fuchs, H., Acir, I.-H., Bohn, B., Brauers, T., Dorn, H.-P., Häsel, R., Hofzumahaus, A., Holland, F., Kaminski, M., Li, X., Lu, K., Lutz, A., Nehr, S., Rohrer, F., Tillmann, R., Wegener, R., and Wahner, A.: OH regeneration from methacrolein oxidation investigated in the atmosphere simulation chamber SAPHIR, *Atmos. Chem. Phys.*, 14, 7895–7908, <https://doi.org/10.5194/acp-14-7895-2014>, 2014.
- Fuchs, H., Novelli, A., Rolletter, M., Hofzumahaus, A., Pfannerstill, E. Y., Kessel, S., Edtbauer, A., Williams, J., Michoud, V., Dusanter, S., Locoge, N., Zannoni, N., Gros, V., Truong, F., Sarda-Esteve, R., Cryer, D. R., Brumby, C. A., Whalley, L. K., Stone, D., Seakins, P. W., Heard, D. E., Schoemaeker, C., Blocquet, M., Coudert, S., Batut, S., Fittschen, C., Thames, A. B., Brune, W. H., Ernest, C., Harder, H., Müller, J. B. A., Elste, T., Kubistin, D., Andres, S., Bohn, B., Hohaus, T., Holland, F., Li, X., Rohrer, F., Kiendler-Scharr, A., Tillmann, R., Wegener, R., Yu, Z., Zou, Q., and Wahner, A.: Comparison of OH reactivity measurements in the atmospheric simulation chamber SAPHIR, *Atmos. Meas. Tech.*, 10, 4023–4053, <https://doi.org/10.5194/amt-10-4023-2017>, 2017.
- 745
- 750
- Glowania, M., Rohrer, F., Dorn, H.-P., Hofzumahaus, A., Holland, F., Kiendler-Scharr, A., Wahner, A., and Fuchs, H.: Comparison of formaldehyde measurements by Hantzsch, CRDS and DOAS in the SAPHIR chamber, *Atmos. Meas. Tech.*, 14, 4239–4253, <https://doi.org/10.5194/amt-14-4239-2021>, 2021.
- 755
- Griffin, R. J., Cocker, D. R., Flagan, R. C., and Seinfeld, J. H.: Organic aerosol formation from the oxidation of biogenic hydrocarbons, *J. Geophys. Res.*, 104, 3555–3567, <https://doi.org/10.1029/1998JD100049>, 1999.



- 760 Guenther, A. B., Jiang, X., Heald, C. L., Sakulyanontvittaya, T., Duhl, T., Emmons, L. K., and Wang, X.: The Model of Emissions of Gases and Aerosols from Nature version 2.1 (MEGAN2.1): an extended and updated framework for modeling biogenic emissions, *Geosci. Model Dev.*, 5, 1471–1492, <https://doi.org/10.5194/gmd-5-1471-2012>, 2012.
- Hakola, H., Arey, J., Aschmann, S. M., and Atkinson, R.: Product formation from the gas-phase reactions of OH radicals and O<sub>3</sub> with a series of monoterpenes, *J. Atmos. Chem.*, 18, 75–102, <https://doi.org/10.1007/BF00694375>, 1994.
- 765 Hakola, H., Rinne, J., and Laurila, T.: The hydrocarbon emission rates of tea-leafed willow (*Salix phylicifolia*), silver birch (*Betula pendula*) and European aspen (*Populus tremula*), *Atmos. Environ.*, 32, 1825–1833, [https://doi.org/10.1016/S1352-2310\(97\)00482-2](https://doi.org/10.1016/S1352-2310(97)00482-2), 1998.
- Hakola, H., Tarvainen, V., Laurila, T., Hiltunen, V., Hellén, H., and Keronen, P.: Seasonal variation of VOC concentrations above a boreal coniferous forest, *Atmos. Environ.*, 37, 1623–1634, [https://doi.org/10.1016/S1352-2310\(03\)00014-1](https://doi.org/10.1016/S1352-2310(03)00014-1), 2003.
- 770 Hantschke, L., Novelli, A., Bohn, B., Cho, C., Reimer, D., Rohrer, F., Tillmann, R., Glowania, M., Hofzumahaus, A., Kiendler-Scharr, A., Wahner, A., and Fuchs, H.: Atmospheric photooxidation and ozonolysis of  $\Delta^3$ -carene and 3-caronaldehyde: rate constants and product yields, *Atmos. Chem. Phys.*, 21, 12665–12685, <https://doi.org/10.5194/acp-21-12665-2021>, 2021.
- Hofzumahaus, A., Rohrer, F., Lu, K., Bohn, B., Brauers, T., Chang, C.-C., Fuchs, H., Holland, F., Kita, K., Kondo, Y., Li, X., Lou, S., Shao, M., Zeng, L., Wahner, A., and Zhang, Y.: Amplified Trace Gas Removal in the Troposphere, *Science*, 324, 1702–1704, <https://doi.org/10.1126/science.1164566>, 2009.
- 775 Holzke, C., Dindorf, T., Kesselmeier, J., Kuhn, U., and Kopppmann, R.: Terpene emissions from European beech (shape *Fagus sylvatica*~L.): Pattern and Emission Behaviour Over two Vegetation Periods, *J. Atmos. Chem.*, 55, 81–102, <https://doi.org/10.1007/s10874-006-9027-9>, 2006.
- Jenkin, M. E., Valorso, R., Aumont, B., Rickard, A. R., and Wallington, T. J.: Estimation of rate coefficients and branching ratios for gas-phase reactions of OH with aliphatic organic compounds for use in automated mechanism construction, *Atmos. Chem. Phys.*, 18, 9297–9328, <https://doi.org/10.5194/acp-18-9297-2018>, 2018.
- 780 Jenkin, M. E., Valorso, R., Aumont, B., Newland, M. J., and Rickard, A. R.: Estimation of rate coefficients for the reactions of O<sub>3</sub> with unsaturated organic compounds for use in automated mechanism construction, *Atmos. Chem. Phys.*, 20, 12921–12937, <https://doi.org/10.5194/acp-20-12921-2020>, 2020.
- 785 Kaminski, M., Fuchs, H., Acir, I.-H., Bohn, B., Brauers, T., Dorn, H.-P., Häseler, R., Hofzumahaus, A., Li, X., Lutz, A., Nehr, S., Rohrer, F., Tillmann, R., Vereecken, L., Wegener, R., and Wahner, A.: Investigation of the  $\alpha$ -pinene photooxidation by OH in the atmosphere simulation chamber SAPHIR, *Atmos. Chem. Phys.*, 17, 6631–6650, <https://doi.org/10.5194/acp-17-6631-2017>, 2017.

- 790 Kim, J.-C., Kim, K.-J., Kim, D.-S., and Han, J.-S.: Seasonal variations of monoterpene emissions from coniferous trees of  
different ages in Korea, *Chemosphere*, 59, 1685–1696, <https://doi.org/10.1016/j.chemosphere.2004.10.048>,  
2005.
- 795 Kuwata, K. T., Luu, L., Weberg, A. B., Huang, K., Parsons, A. J., Peebles, L. A., Rackstraw, N. B., and Kim, M. J.: Quantum  
Chemical and Statistical Rate Theory Studies of the Vinyl Hydroperoxides Formed in *trans*-2-Butene and  
2,3-Dimethyl-2-butene Ozonolysis, *J. Phys. Chem. A*, 122, 2485–2502,  
<https://doi.org/10.1021/acs.jpca.8b00287>, 2018.
- Larsen, Bo. R., Di Bella, D., Glasius, M., Winterhalter, R., Jensen, N. R., and Hjorth, J.: Gas-Phase OH Oxidation of  
Monoterpenes: Gaseous and Particulate Products, *J. Atmos. Chem.*, 38, 231–276,  
<https://doi.org/10.1023/A:1006487530903>, 2001.
- 800 Lee, A., Goldstein, A. H., Kroll, J. H., Ng, N. L., Varutbangkul, V., Flagan, R. C., and Seinfeld, J. H.: Gas-phase products and  
secondary aerosol yields from the photooxidation of 16 different terpenes, *J. Geophys. Res.*, 111, D17305,  
<https://doi.org/10.1029/2006JD007050>, 2006.
- Lelieveld, J., Butler, T. M., Crowley, J. N., Dillon, T. J., Fischer, H., Ganzeveld, L., Harder, H., Lawrence, M. G., Martinez,  
M., Taraborrelli, D., and Williams, J.: Atmospheric oxidation capacity sustained by a tropical forest, *Nature*,  
452, 737–740, <https://doi.org/10.1038/nature06870>, 2008.
- 805 Long, B., Bao, J. L., and Truhlar, D. G.: Atmospheric Chemistry of Criegee Intermediates: Unimolecular Reactions and  
Reactions with Water, *J. Am. Chem. Soc.*, 138, 14409–14422, <https://doi.org/10.1021/jacs.6b08655>, 2016.
- Lou, S., Holland, F., Rohrer, F., Lu, K., Bohn, B., Brauers, T., Chang, C. C., Fuchs, H., Häseler, R., Kita, K., Kondo, Y., Li,  
X., Shao, M., Zeng, L., Wahner, A., Zhang, Y., Wang, W., and Hofzumahaus, A.: Atmospheric OH  
reactivities in the Pearl River Delta – China in summer 2006: measurement and model results, *Atmos. Chem.*  
810 *Phys.*, 10, 11243–11260, <https://doi.org/10.5194/acp-10-11243-2010>, 2010.
- Ma, Y. and Marston, G.: Multifunctional acid formation from the gas-phase ozonolysis of  $\beta$ -pinene, *Phys. Chem. Chem. Phys.*,  
10, 6115, <https://doi.org/10.1039/b807863g>, 2008.
- Mellouki, A., Ammann, M., Cox, R. A., Crowley, J. N., Herrmann, H., Jenkin, M. E., McNeill, V. F., Troe, J., and Wallington,  
T. J.: Evaluated kinetic and photochemical data for atmospheric chemistry: volume VIII – gas-phase  
815 reactions of organic species with four, or more, carbon atoms ( $\geq C_4$ ), *Atmos. Chem. Phys.*, 21, 4797–4808,  
<https://doi.org/10.5194/acp-21-4797-2021>, 2021.
- Nguyen, T. B., Tyndall, G. S., Crouse, J. D., Teng, A. P., Bates, K. H., Schwantes, R. H., Coggon, M. M., Zhang, L., Feiner,  
P., Miller, D. O., Skog, K. M., Rivera-Rios, J. C., Dorris, M., Olson, K. F., Koss, A., Wild, R. J., Brown, S.  
S., Goldstein, A. H., de Gouw, J. A., Brune, W. H., Keutsch, F. N., Seinfeld, J. H., and Wennberg, P. O.:  
820 Atmospheric fates of Criegee intermediates in the ozonolysis of isoprene, *Phys. Chem. Chem. Phys.*, 18,  
10241–10254, <https://doi.org/10.1039/C6CP00053C>, 2016.

- Nguyen, T. L., Peeters, J., and Vereecken, L.: Theoretical study of the gas-phase ozonolysis of  $\beta$ -pinene ( $C_{10}H_{16}$ ), *Phys. Chem. Chem. Phys.*, 11, 5643, <https://doi.org/10.1039/b822984h>, 2009.
- 825 Novelli, A., Vereecken, L., Bohn, B., Dorn, H.-P., Gkatzelis, G. I., Hofzumahaus, A., Holland, F., Reimer, D., Rohrer, F., Rosanka, S., Taraborrelli, D., Tillmann, R., Wegener, R., Yu, Z., Kiendler-Scharr, A., Wahner, A., and Fuchs, H.: Importance of isomerization reactions for OH radical regeneration from the photo-oxidation of isoprene investigated in the atmospheric simulation chamber SAPHIR, *Atmos. Chem. Phys.*, 20, 3333–3355, <https://doi.org/10.5194/acp-20-3333-2020>, 2020.
- 830 Novelli, A., Pang, J. Y. S., Färber, M., Carlsson, P. T. M., Bohn, B., Gkatzelis, G. I., Rohrer, F., Wedel, S., and Fuchs, H.: Atmospheric simulation chamber study: Sabinene +  $O_3$  - Gas-phase oxidation - kinetic study (1.0), <https://doi.org/10.25326/W4QV-KY95>, 2023a.
- Novelli, A., Pang, J. Y. S., Färber, M., Carlsson, P. T. M., Bohn, B., Gkatzelis, G. I., Rohrer, F., Wedel, S., and Fuchs, H.: Atmospheric simulation chamber study: Sabinene +  $O_3$  - Gas-phase oxidation - kinetic study (1.0), <https://doi.org/10.25326/8BA6-MM58>, 2023b.
- 835 Novelli, A., Pang, J. Y. S., Färber, M., Carlsson, P. T. M., Bohn, B., Gkatzelis, G. I., Rohrer, F., Wedel, S., and Fuchs, H.: Atmospheric simulation chamber study: Sabinene + OH - Gas-phase oxidation - kinetic study (1.0), <https://doi.org/10.25326/QDQE-8Q79>, 2023c.
- Novelli, A., Pang, J. Y. S., Färber, M., Carlsson, P. T. M., Bohn, B., Gkatzelis, G. I., Rohrer, F., Wedel, S., and Fuchs, H.: Atmospheric simulation chamber study: Sabinene + OH - Gas-phase oxidation - kinetic study (1.0), <https://doi.org/10.25326/25V8-PA77>, 2023d.
- 840 Novelli, A., Pang, J. Y. S., Färber, M., Carlsson, P. T. M., Bohn, B., Gkatzelis, G. I., Rohrer, F., Wedel, S., and Fuchs, H.: Atmospheric simulation chamber study: Sabinene + OH - Gas-phase oxidation - kinetic study (1.0), <https://doi.org/10.25326/FCYS-Y288>, 2023e.
- Novelli, A., Pang, J. Y. S., Färber, M., Carlsson, P. T. M., Bohn, B., Gkatzelis, G. I., Rohrer, F., Wedel, S., and Fuchs, H.: Atmospheric simulation chamber study: Sabinene + OH - Gas-phase oxidation - kinetic study (1.0), <https://doi.org/10.25326/B5VV-K378>, 2023f.
- 845 Novelli, A., Pang, J. Y. S., Färber, M., Carlsson, P. T. M., Bohn, B., Gkatzelis, G. I., Rohrer, F., Wedel, S., and Fuchs, H.: Atmospheric simulation chamber study: Sabinene + OH - Gas-phase oxidation - kinetic study (1.0), <https://doi.org/10.25326/BQVM-QR53>, 2023g.
- 850 Pang, J. Y. S., Novelli, A., Kaminski, M., Acir, I.-H., Bohn, B., Carlsson, P. T. M., Cho, C., Dorn, H.-P., Hofzumahaus, A., Li, X., Lutz, A., Nehr, S., Reimer, D., Rohrer, F., Tillmann, R., Wegener, R., Kiendler-Scharr, A., Wahner, A., and Fuchs, H.: Investigation of the limonene photooxidation by OH at different NO concentrations in the atmospheric simulation chamber SAPHIR (Simulation of Atmospheric PHotochemistry In a large Reaction Chamber), *Atmos. Chem. Phys.*, 22, 8497–8527, <https://doi.org/10.5194/acp-22-8497-2022>, 2022.

- 855 Peeters, J., Boullart, W., Pultau, V., Vandenberk, S., and Vereecken, L.: Structure–Activity Relationship for the Addition of OH to (Poly)alkenes: Site-Specific and Total Rate Constants, *J. Phys. Chem. A*, 111, 1618–1631, <https://doi.org/10.1021/jp066973o>, 2007.
- Peeters, J., Müller, J.-F., Stavrou, T., and Nguyen, V. S.: Hydroxyl Radical Recycling in Isoprene Oxidation Driven by Hydrogen Bonding and Hydrogen Tunneling: The Upgraded LIM1 Mechanism, *J. Phys. Chem. A*, 118, 8625–8643, <https://doi.org/10.1021/jp5033146>, 2014.
- 860 Pfeifle, M., Ma, Y.-T., Jasper, A. W., Harding, L. B., Hase, W. L., and Klippenstein, S. J.: Nascent energy distribution of the Criegee intermediate CH<sub>2</sub>OO from direct dynamics calculations of primary ozonide dissociation, *The Journal of Chemical Physics*, 148, 174306, <https://doi.org/10.1063/1.5028117>, 2018.
- Reissell, A., Harry, C., Aschmann, S. M., Atkinson, R., and Arey, J.: Formation of acetone from the OH radical- and O<sub>3</sub>-initiated reactions of a series of monoterpenes, *J. Geophys. Res.*, 104, 13869–13879, <https://doi.org/10.1029/1999JD900198>, 1999.
- 865 Rohrer, F., Bohn, B., Brauers, T., Brüning, D., Johnen, F.-J., Wahner, A., and Kleffmann, J.: Characterisation of the photolytic HONO-source in the atmosphere simulation chamber SAPHIR, *Atmos. Chem. Phys.*, 5, 2189–2201, <https://doi.org/10.5194/acp-5-2189-2005>, 2005.
- 870 Rolletter, M., Kaminski, M., Acir, I.-H., Bohn, B., Dorn, H.-P., Li, X., Lutz, A., Nehr, S., Rohrer, F., Tillmann, R., Wegener, R., Hofzumahaus, A., Kiendler-Scharr, A., Wahner, A., and Fuchs, H.: Investigation of the  $\alpha$ -pinene photooxidation by OH in the atmospheric simulation chamber SAPHIR, *Atmos. Chem. Phys.*, 19, 11635–11649, <https://doi.org/10.5194/acp-19-11635-2019>, 2019.
- Rollins, A. W., Smith, J. D., Wilson, K. R., and Cohen, R. C.: Real Time In Situ Detection of Organic Nitrates in Atmospheric Aerosols, *Environ. Sci. Technol.*, 44, 5540–5545, <https://doi.org/10.1021/es100926x>, 2010.
- 875 Sekimoto, K., Li, S.-M., Yuan, B., Koss, A., Coggon, M., Warneke, C., and De Gouw, J.: Calculation of the sensitivity of proton-transfer-reaction mass spectrometry (PTR-MS) for organic trace gases using molecular properties, *Int. J. Mass Spectrom.*, 421, 71–94, <https://doi.org/10.1016/j.ijms.2017.04.006>, 2017.
- da Silva, G., Graham, C., and Wang, Z.-F.: Unimolecular  $\beta$ -Hydroxyperoxy Radical Decomposition with OH Recycling in the Photochemical Oxidation of Isoprene, *Environ. Sci. Technol.*, 44, 250–256, <https://doi.org/10.1021/es900924d>, 2010.
- 880 Sindelarova, K., Granier, C., Bouarar, I., Guenther, A., Tilmes, S., Stavrou, T., Stefani, P., and Knorr, W.: Global data set of biogenic VOC emissions calculated by the MEGAN model over the last 30 years, *Atmos. Chem. Phys.*, 25, <https://doi.org/10.5194/acp-14-9317-2014>, 2014.
- 885 Staudt, M. and Bertin, N.: Light and temperature dependence of the emission of cyclic and acyclic monoterpenes from holm oak (*Quercus ilex* L.) leaves, *Plant Cell Environ.*, 21, 385–395, <https://doi.org/10.1046/j.1365-3040.1998.00288.x>, 1998.

- Tollsten, L. and Müller, P. M.: Volatile organic compounds emitted from beech leaves, *Phytochem.*, 43, 759–762, [https://doi.org/10.1016/0031-9422\(96\)00272-5](https://doi.org/10.1016/0031-9422(96)00272-5), 1996.
- 890 Vereecken, L. and Nozière, B.: H migration in peroxy radicals under atmospheric conditions, *Atmos. Chem. Phys.*, 20, 7429–7458, <https://doi.org/10.5194/acp-20-7429-2020>, 2020.
- Vereecken, L. and Peeters, J.: A theoretical study of the OH-initiated gas-phase oxidation mechanism of  $\beta$ -pinene ( $C_{10}H_{16}$ ): first generation products, *Phys. Chem. Chem. Phys.*, 14, 3802, <https://doi.org/10.1039/c2cp23711c>, 2012.
- Vereecken, L., Novelli, A., and Taraborrelli, D.: Unimolecular decay strongly limits the atmospheric impact of Criegee intermediates, *Phys. Chem. Chem. Phys.*, 19, 31599–31612, <https://doi.org/10.1039/C7CP05541B>, 2017.
- 895 Wang, L. and Wang, L.: Mechanism of gas-phase ozonolysis of sabinene in the atmosphere, *Phys. Chem. Chem. Phys.*, 19, 24209–24218, <https://doi.org/10.1039/C7CP03216A>, 2017.
- Wang, L. and Wang, L.: Atmospheric Oxidation Mechanism of Sabinene Initiated by the Hydroxyl Radicals, *J. Phys. Chem. A*, 122, 8783–8793, <https://doi.org/10.1021/acs.jpca.8b06381>, 2018.
- 900 Whalley, L. K., Edwards, P. M., Furneaux, K. L., Goddard, A., Ingham, T., Evans, M. J., Stone, D., Hopkins, J. R., Jones, C. E., Karunaharan, A., Lee, J. D., Lewis, A. C., Monks, P. S., Moller, S. J., and Heard, D. E.: Quantifying the magnitude of a missing hydroxyl radical source in a tropical rainforest, *Atmos. Chem. Phys.*, 11, 7223–7233, <https://doi.org/10.5194/acp-11-7223-2011>, 2011.
- Xu, L., Møller, K. H., Crouse, J. D., Otkjær, R. V., Kjaergaard, H. G., and Wennberg, P. O.: Unimolecular Reactions of Peroxy Radicals Formed in the Oxidation of  $\alpha$ -Pinene and  $\beta$ -Pinene by Hydroxyl Radicals, *J. Phys. Chem. A*, 123, 1661–1674, <https://doi.org/10.1021/acs.jpca.8b11726>, 2019.
- 905 Yu, J., Cocker III, D. R., Griffin, R. J., Flagan, R. C., and Seinfeld, J. H.: Gas-Phase Ozone Oxidation of Monoterpenes: Gaseous and Particulate Products, *J. Atmos. Chem.*, 34, 207–258, <https://doi.org/10.1023/A:1006254930583>, 1999.

910